Appendix B–Small Beam Tests

Table of Contents

List of Figures

List of Tables

1   Introduction

The AASHTO LRFD Bridge Design Specifications (2007) require that confinement reinforcement be placed around prestressing strands in the bottom bulb of pretensioned concrete beams. Although the AASHTO specifications contain prescriptive requirements for the quantity and placement of confinement reinforcement, the effect of such reinforcement on the end region behavior is not well understood.

To evaluate the function and effect of confinement reinforcement, load tests were conducted using 28-in. deep precast-pretensioned beams. In total, twelve tests were conducted with each specimen loaded in three-point bending at a shear span-to-depth ratio of 1.0. Load, displacement, and strain data were collected during each test. Variables in the test program included strand size, strand quantity, prestressing force, and the presence or lack of confinement reinforcement.

Goals of the test program described in this chapter include:

- Evaluate the effect(s) of confinement reinforcement on specimen capacity and behavior
- Evaluate the interaction(s) between confinement reinforcement and other test variables
- Compile load, strain, and displacement data for use in validating finite element models (See Appendix F)
- Evaluate transverse strain distribution in the bottom flange above the bearing.

Relevant literature is summarized in Appendix A.

2   Beam History

Beams used in the test program were initially fabricated for use in project by O'Neill and Hamilton (2009). The initial test program focused on flexural behavior only, and did not damage the end region of the beams where shear tests were performed the current project. Six beams were fabricated at a precast facility in Leesburg, FL, and then shipped to the FDOT Structures Laboratory in Tallahassee, FL where a cast-in-place deck was added to each beam. After the cast-in-place decks were sufficiently cured, flexural testing by O'Neill and Hamilton was conducted, also at the FDOT Structures Laboratory.

The beams were originally constructed with confinement reinforcement at both ends. After the initial flexural testing by O'Neill and Hamilton, the beams were modified prior to conducting shear tests. This modification consisted of removing the portion containing confinement reinforcement from one end of each beam (Figure 1). Following the modification, shear tests were conducted on each end of each beam resulting in (12) total shear tests. For purposes of this report, each end will be referred to as a separate test specimen.
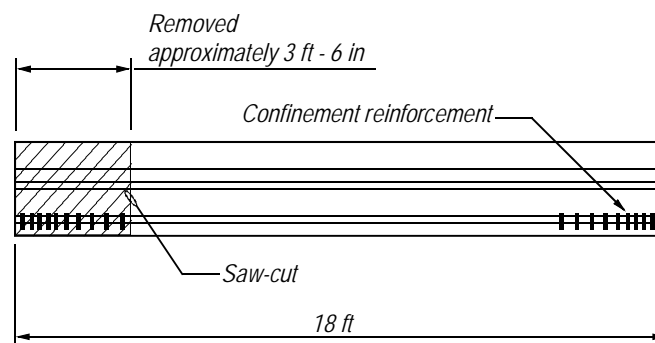
Figure 1–Small beam modification

3 Beam Design

The beam cross section dimensions are shown in Figure 2. Each beam was reinforced with single-leg #4 stirrups at 3 in. o.c. throughout all but the center 3 ft of the beam (Figure 3). Confinement reinforcement consisted of (10) #3 hoops in the end region as shown in Figure 3. An 8 in. thick by 18 in. wide deck was added to the top of each beam. The deck was reinforced with #5 bars longitudinally and transversely as shown in Figure 4.
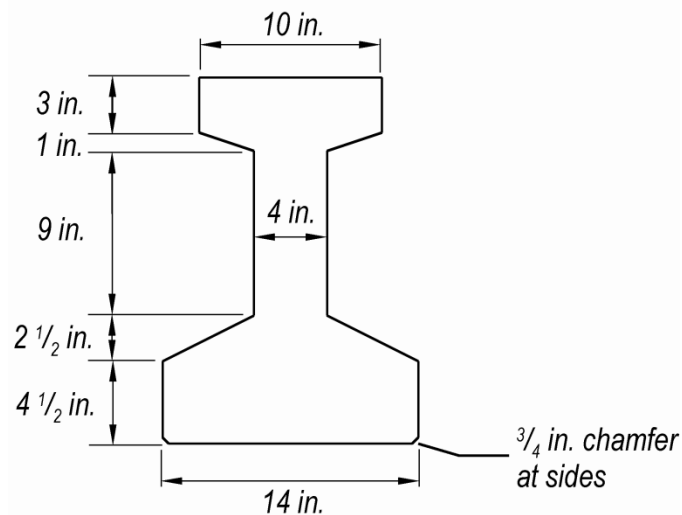
Figure 2–Cross-section dimensions of all test beams
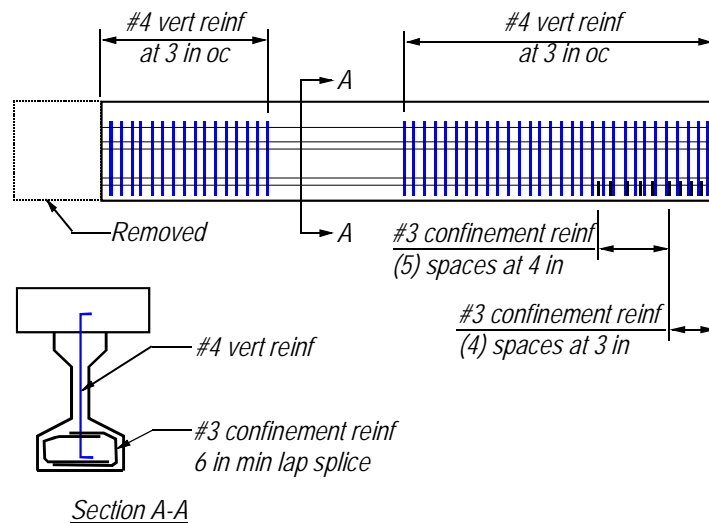
Figure 3–Vertical and confinement reinforcement
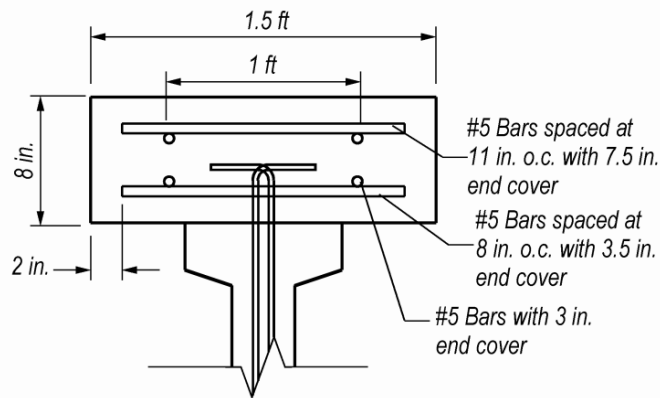
Figure 4–Deck dimensions and reinforcement layout

Three variables were considered in the small beam test program: 1) Strand size, 2) Strand quantity, and 3) Presences or lack of confinement reinforcement. Each variable is denoted in the test nomenclature shown in Figure 5.
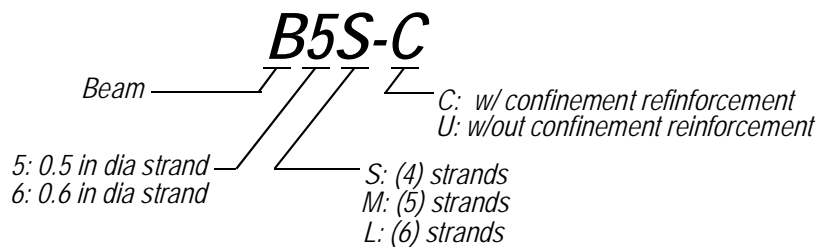
Figure 5–Small beam test nomenclature

Figure 6 shows the three strand patterns used in the specimen design. B5S, B5M, B5L were prestressed with 0.5-in. diameter ASTM A416 seven-wire strand and B6S, B6M, B6L were prestressed with 0.6-in. diameter strand. The 0.5-in. and 0.6-in. prestressing strands were initially stressed to 50% and 74% of the ultimate strength (270-ksi), respectively.
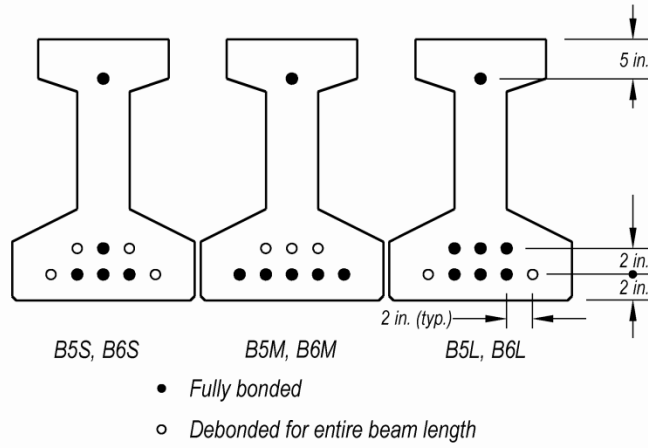
Figure 6–Strand layouts for beams containing 0.5-in. and 0.6-in. strand

4   Beam Construction and Material Properties

Beams B5S, B5M, and B5L were cast from a single batch of concrete. Similarly, beams B6S, B6M, and B6L were also cast from a single mixing batch. The same mix design was used for both batches. The mix contained 90% of granite aggregate equal to or less than 3/8 in. with no aggregates exceeding 0.5 in. For each batch (9) 6 x 12 in. cylinders for compressive strength and modulus of elasticity testing were taken. Additionally, the producer cast 4 x 8 in. cylinders for determining release strength and 28-day compressive strength.

Table 1 shows the cylinder test results at release and at 28-days. Each value is the average of three tests. The design called for a release strength of 3500 psi, which was reached within one day of casting. The B6x beams, however, were not released until four days after casting due to construction scheduling. Note the average 28-day compressive strength from the 6 x 12 in. cylinders is not provided for the B6x. The test machine was thought to have malfunctioned during these cylinder tests, and that the producer tests conducted at 28-day age are a better estimate of the compressive strength.

Table 1–Results for compressive strength and modulus of rupture tests (psi)

Beams	6 x 12 in. cylinders		4 x 8 in. cylinders (Manufacturer)	
	Release*	28 day**	Release*	28 day**
B5x	3900	8400	3980	9750
B6x	5370	N/A	4902	8840

*f'_{ci} = 3500 psi ** f'_c = 6000 psi

An FDOT Class II concrete deck was cast on each beam (f'_c = 4500 psi) after they were delivered to the FDOT Structural Research Center. Figure 7 shows the completed test beams.

Figure 7–Finished beam specimens ready for testing

5   Test Setup and Instrumentation

Load tests were conducted on each end of all six beams, resulting in twelve total tests. For purposes of this report, each end will be referred to as an individual test specimen. Tests were conducted using a three-point loading scheme (Figure 8, Figure 9). The end of the beam not being tested was cantilevered beyond the far support. After the first specimen (end) was tested, the supports and load point were moved and the second specimen was tested. One end of each beam had confinement reinforcement and one end did not. The specimen with confinement reinforcement was tested first in all cases except for B6M-U and B6M-C, for which the unconfined specimen was tested first.
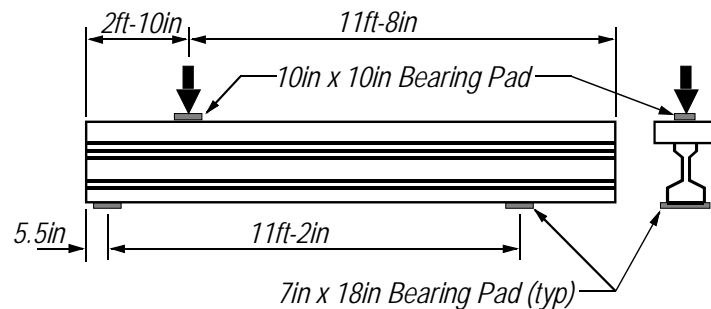
Figure 8–Small beam test setup
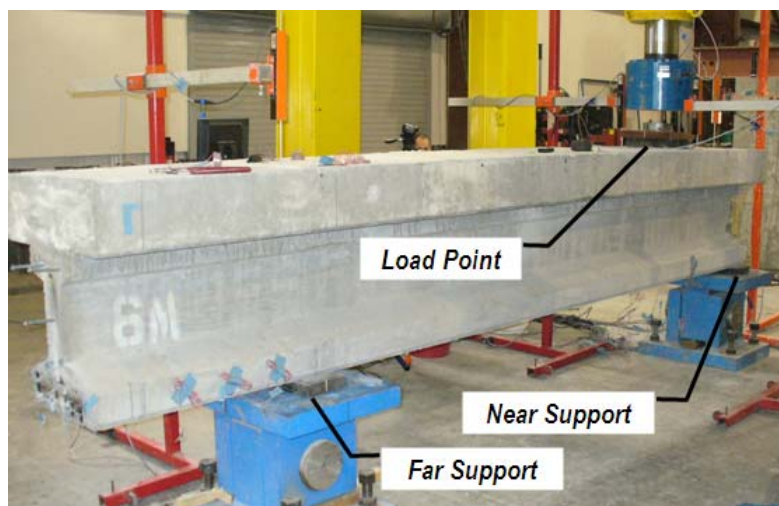
Figure 9–Specimen prior to load test

Beams were supported on 2-in. thick x 7 in. x 18 in. reinforced neoprene bearing pads with the pad oriented such that the 18 in. dimension was perpendicular to the beam axis (Figure 10). Load was applied through a 2-in. thick x 10 in. x 10 in. reinforced bearing pad (Figure 11) at a rate of 0.25 kip/sec. The load was measured by a load cell at the point of application.

Figure 10–Specimen on bearing pad

Figure 11–Load point

Linear variable displacement transducers, LVDTs, were used to measure vertical displacement at the load point, at each support (Figure 12), and to measure strand slip at the end of the beams (Figure 13). A wood frame was used to position the LVDTs at the end of the beam (Figure 14). Electrical resistance foil strain gages recorded strain at discrete locations on the test

beams (Figure 15). Gages were typically 60-mm long, however 30 mm gages were used to measure transverse strain at the end of the beam (S6-S10). Figure 16 shows specimen B6S-C during testing. The load and support points are shown along with strain gage S2 and the LVDTs monitoring strand slip.
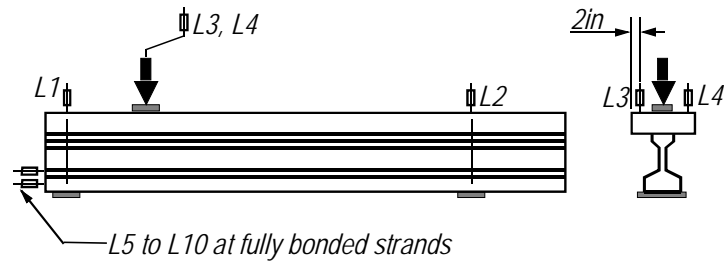
Figure 12–Small beam LVDT placement
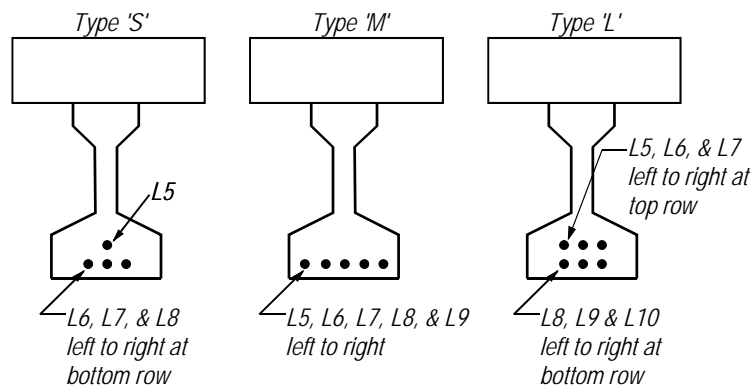
Figure 13–LVDTs at strands
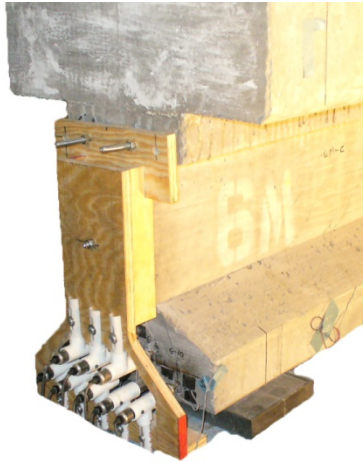
Figure 14–LVDT frame at end of beam
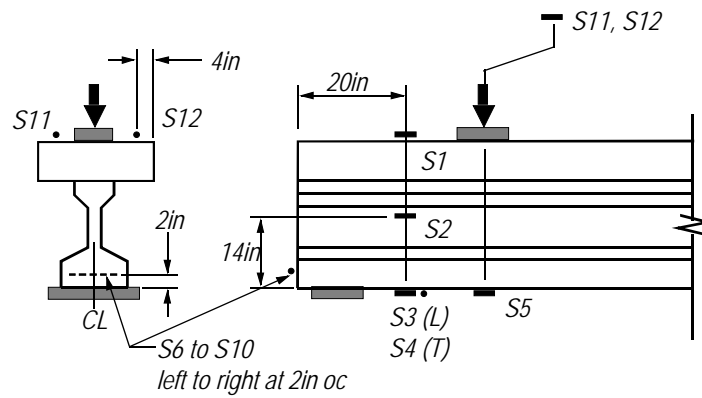
Figure 15–Strain gage placement

Figure 16–Specimen during testing

6   Results and Discussion

Confinement reinforcement was the most significant variable that affected the shear capacity and behavior. As such, test results are presented in pairs of similar confined and unconfined specimens in the following sections. For each pairing, the confined specimen and unconfined specimens were located on opposite ends of the same beam. Because the same beam was used for both tests in each pairing, both specimens had the same prestressing force, strand quantity, and strand pattern.   For example, specimens B5L-C and B5L-U each had (6) 0.5-in. diameter strands, and were located at opposite ends of the same beam.

For convenience in reporting test results, the supports are referred to as the "near support" and the "far support." The near support is the support closest to the load point, and the far support is farthest from the load point.

A summary figure is presented for each pairing of specimens. Each summary figure presents the load-displacement and load-slip results, first and final cracks locations, maximum load, displacement ductility, and failure mode. The displacement shown in the figures is the displacement at the load point, and has been adjusted to remove the effect of the bearing pad displacement. Strand slip presented in the test summaries are the average slip of each fully bonded strand as measured at the near support. Displacement ductility was calculated as the displacement at maximum load divided by the displacement at the on-set of nonlinearity as determined visually from the load-displacement diagram.

Three types of failures were observed in the beam tests: splitting, bond-flexure, and bond-shear. Failure modes and characteristics are presented in Table 2. Photos of specimens with different failure modes are shown in Figure 17 through Figure 20.

Table 2–Failure modes

Failure Mode	No. of Specimens	Characteristics
Splitting	6	Peak capacity is governed by the formation of a splitting crack above the support. Strands cannot support tensile force after formation of splitting crack.
Bond-Flexure	2	Strand slip after the formation of cracks. Peak capacity is governed by crushing of the compression zone. Deformation and rotation leading to crushing is augmented by the strand slip.
Bond-Shear	3	Strand slip after the formation of cracks. Peak capacity is governed by strand-concrete bond capacity.
Flexural	1	Load-displacement plot reaches a plateau indicating yielding of the reinforcement. Applied moment exceeds nominal moment capacity.
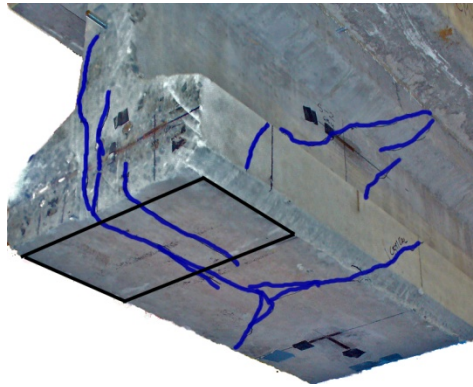
Figure 17–Bottom view of B6M-U with splitting failure mode
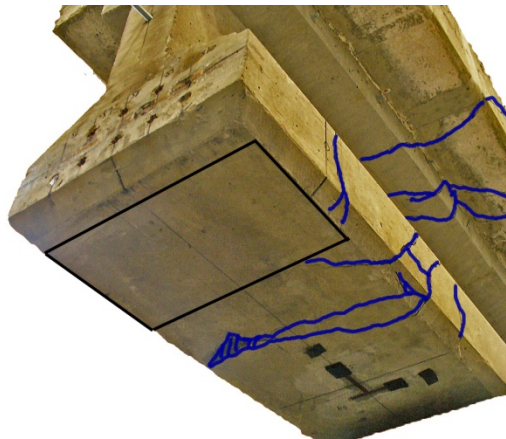
Figure 18–Bottom view of B6L-C with bond-shear failure mode

Figure 19–Bond-flexure failure mode (B6M-C)
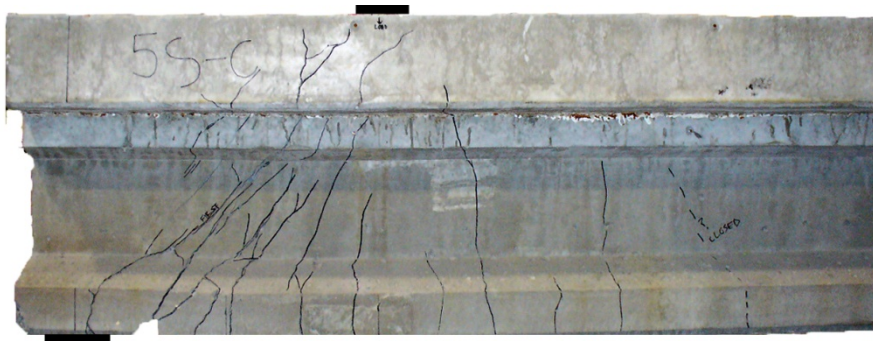
Figure 20–Flexural failure mode (B5S-C)

The specimens used in the testing were constructed and tested under a separate research program (O'Neill and Hamilton 2009), which focused on flexural stresses at mid-span. The beams were loaded in flexure up to and beyond cracking, but not to ultimate flexural capacity. Also, the specimens were modified prior to the current test program by saw-cutting the portion containing confinement reinforcement from one end of each beam (Figure 3). This modification was made to create the unconfined test conditions.

Previous flexural loading of the beams did not result in any visible cracking or damage to the end regions where the shear testing in the current program was focused. Micro-cracking, however, may have formed during the initial load tests and had some influence on the initial cracking loads in the shear tests. Micro-cracks, however, would have had different effects on confined and unconfined specimens. This is because the confined specimen tests used the same

bearing location as the tests by O'Neill and Hamilton, whereas the unconfined tests did not use the same bearing location.

For each pairing of confined and unconfined specimens, cracking always initiated in the confined specimen at a lower load. On average the load at initial cracking was 13% lower in the confined specimens that in the accompanying unconfined specimens. The early cracking in the confined specimens could have been initiated by micro-cracks in the end region that had formed during previous testing. Alternatively, differences in transfer length due to beam modification may also have been a factor influencing the cracking loads. Neither possibility can be evaluated from the available data, however the lower cracking loads in the confined specimens do suggest that the test procedures had some effect on the results. These effects, however, tend to support the results of the test program. For example, the confined specimens cracked at lower loads but still had greater strength and ductility than the unconfined specimens. Consequently, the beam modification and previous testing were concluded to have negligible effect. The FIB-54 girder test program, reported in Appendix D, did not have the same limitations as the small beams and can be used to verify the results and assumptions used in the small beam program.

6.1   B5L-C and B5L-U

Figure 21 summarizes the results for tests B5L-C and B5L-U. Each of these specimens had (6) 0.5 in. diameter strands, and varied only due to the presence or lack of confinement reinforcement. Both specimens behaved linear elastically until the formation of cracks. The first cracks were inclined web cracks occurring between the near support and the load point. Strain data from S2 gages indicated that initial cracks formed at applied loads of 96 kip and 116 kip for B5L-C and B5L-U, respectively. As the load increased, additional cracks formed in each specimen, and the cracks propagated into the flanges and the deck. Stiffness of each specimen was similar throughout loading.

Strands in each specimen began to slip after crack formation. Strands in specimen B5L-C began to slip gradually at an applied load of 96 kip, and more rapidly at load of 170 kip. Strands in B5L-U began to slip gradually at 116 kip and more rapidly at a load of 175 kip. In both cases, rapid strand slip was preceded by the formation of cracks in the bottom bulb that reduced the available development length. Abrupt strand slip in B5L-U occurred at 190 kip in

association with the formation of splitting cracks above the bearing. The strand slip at maximum load was 0.23 in. and 0.03 in. for B5L-C and B5L-U, respectively.

Specimen B5L-U supported a maximum applied load of 190 kip. At this load, a splitting crack formed above the near support and the specimen immediately lost load capacity. Failure of B5L-U was designated as a splitting failure.

Splitting failure did not occur in B5L-C, allowing this specimen to support additional load and displacement beyond the point at which B5L-U failed. Absence of splitting in B5L-C is attributed to the confinement reinforcement that controlled formation of splitting cracks. By preventing splitting, the confinement reinforcement allowed larger loads to be developed in the top strand and vertical reinforcement, which added to the specimen capacity. B5L-C supported a maximum applied load of 226 kip. At this load, testing was terminated because the specimen had almost no stiffness. Slip at peak load was 0.23 in. Continuation of the test would not have resulted in significantly higher load, but would have resulted in additional displacement, rotation, slip, and eventually crushing of the compression zone. Failure of B5L-C is designated as a bond-shear failure.

6.2   B5M-C and B5M-U

Figure 22 summarizes the test results of B5M-C and B5M-U. Each of these specimens had (5) 0.5-in. diameter strands and varied only due to the presence or lack of confinement reinforcement. Both specimens behaved linear elastically until the formation of cracks. The first cracks were inclined cracks occurring in the web between the near support and the load point. Strain data from S2 gages indicate that initial cracks formed at applied loads of 93 kip and 103 kip for B5M-C and B5M-U, respectively. As the load increased, additional cracks formed in each specimen, and the cracks propagated into the flanges and the deck. Stiffness of each specimen was similar throughout loading.
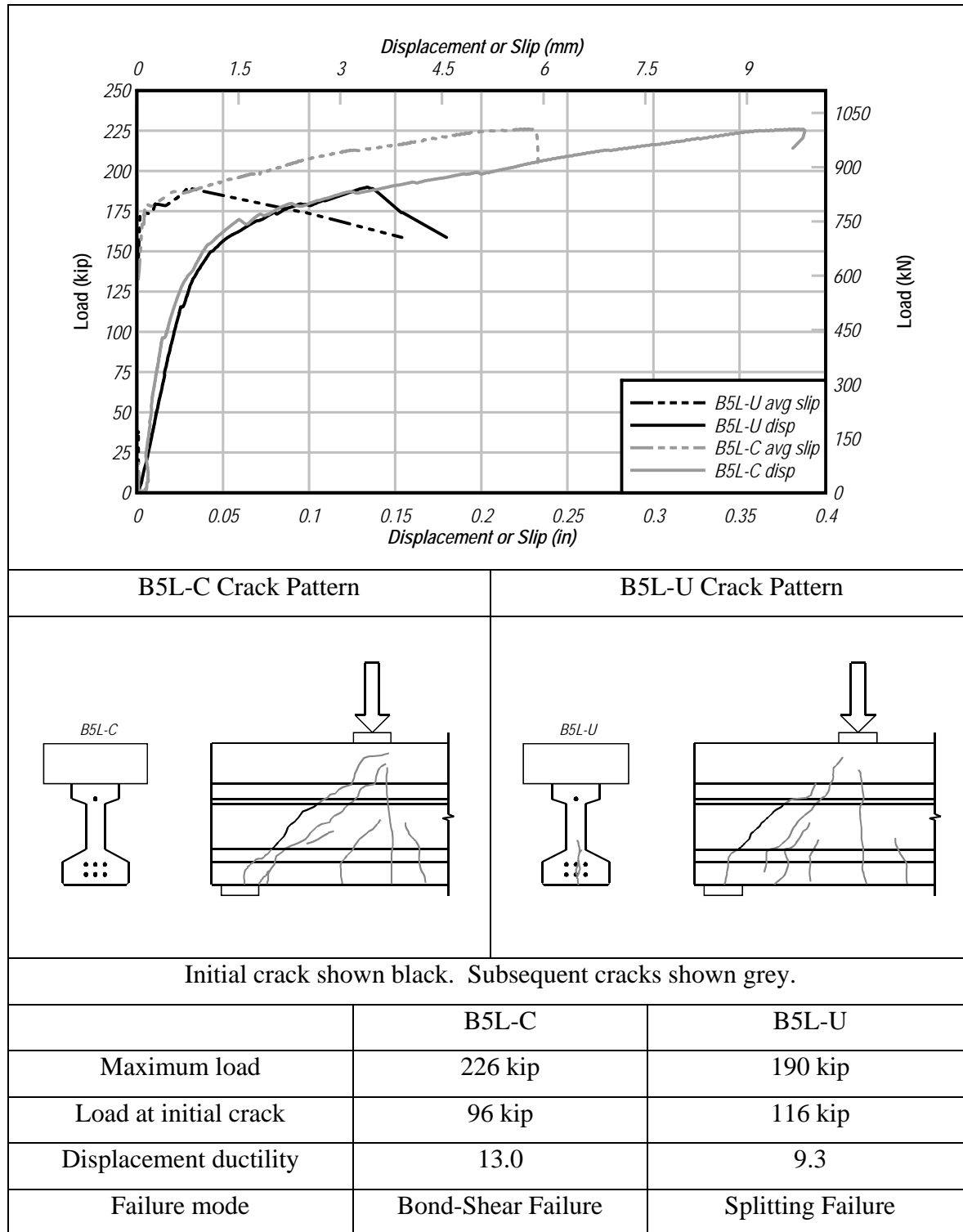
Figure 21–Summary of results for B5L-C and B5L-U

	B5L-C	B5L-U
Maximum load	226 kip	190 kip
Load at initial crack	96 kip	116 kip
Displacement ductility	13.0	9.3
Failure mode	Bond-Shear Failure	Splitting Failure

Strands in each specimen began to slip after the formation of cracks. Strands in specimen B5M-C began to slip gradually at an applied load of 113 kip, and more rapidly at load of 162 kip. Rapid slip at 162 kip occurred simultaneously with spalling of concrete from the bottom bulb. Spalling was limited to concrete outside of the confinement reinforcement. Strands in B5M-U did not slip until a load of 155 kip, by which load cracks had formed in the bottom bulb. Abrupt slip in B5M-U occurred at a load of 180 kip in association with the formation of a splitting crack above the bearing point. The strand slip at maximum load was 0.26 in. and 0.03 in. for B5M-C and B5M-U respectively.

Specimen B5M-U supported as maximum applied load of 180 kip. At this load a splitting crack formed above the near support and the specimen almost instantly lost load capacity. Failure of B5M-U is designated as a splitting failure. Figure__ shows the splitting crack at the end and bottom of B5M-U.

Splitting failure did not occur in B5M-C, allowing this specimen to support additional load and displacement beyond the point at which B5M-U failed. Absence of splitting in B5M-C is attributed to the confinement reinforcement which controlled formation of splitting cracks. By preventing splitting, the confinement reinforcement allowed larger loads to be developed in the top strand and vertical reinforcement, which added to the specimen capacity. B5M-C supported a maximum applied load of 205 kip. At this load, the compression zone on either side of the load point crushed. The rotation that led to compression zone crushing was augmented by strand slip. Failure of B5M-C (Figure 24) is designated as a bond-flexure failure.
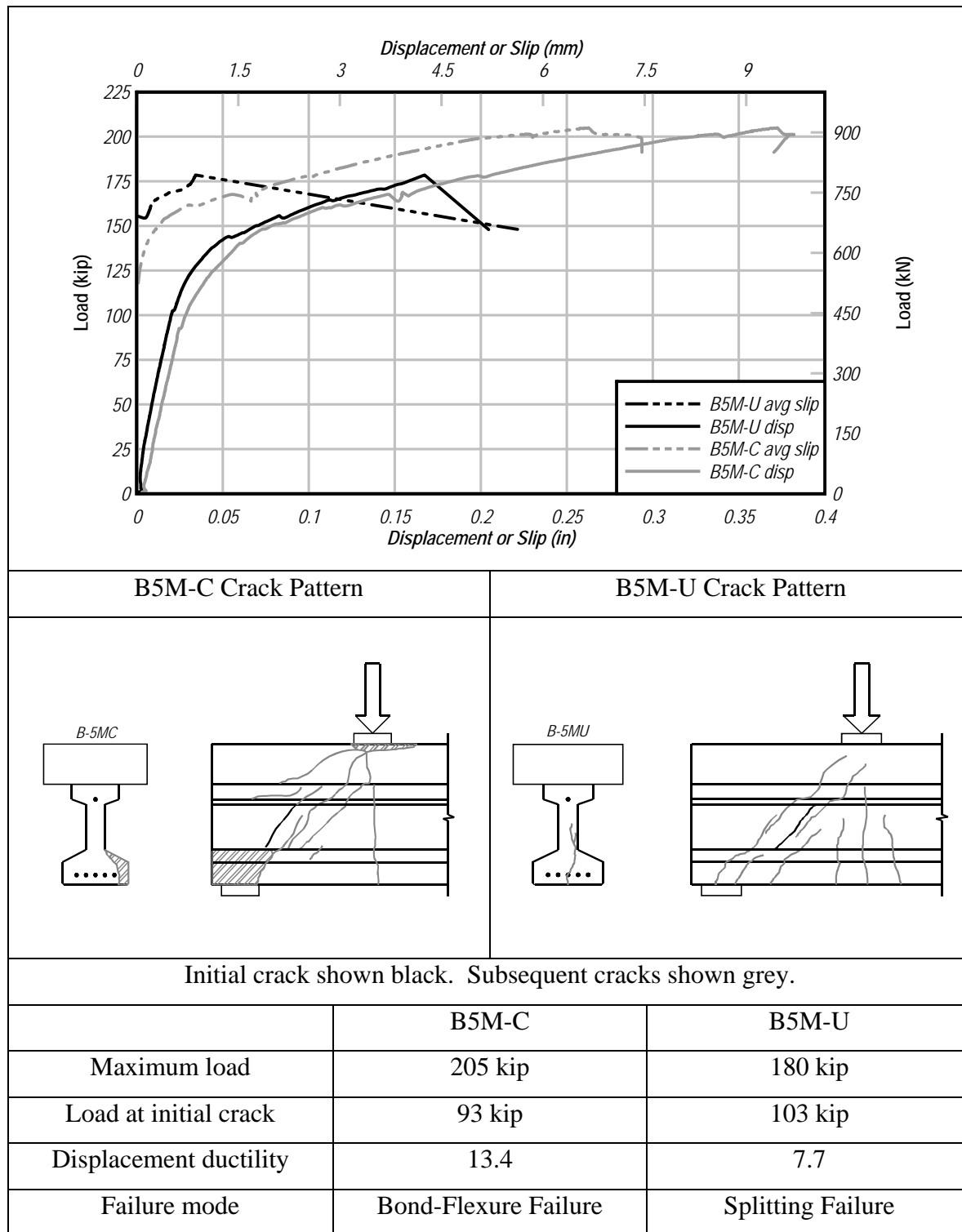
Figure 22–Summary of results for B5M-C and B5M-U

	B5M-C	B5M-U
Maximum load	205 kip	180 kip
Load at initial crack	93 kip	103 kip
Displacement ductility	13.4	7.7
Failure mode	Bond-Flexure Failure	Splitting Failure
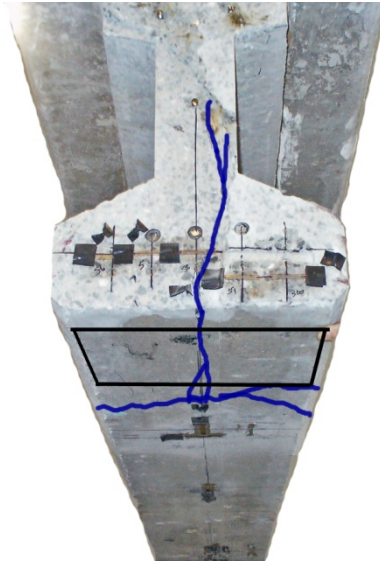
Figure 23–Bottom view of specimen with splitting failure mode (B5M-U)
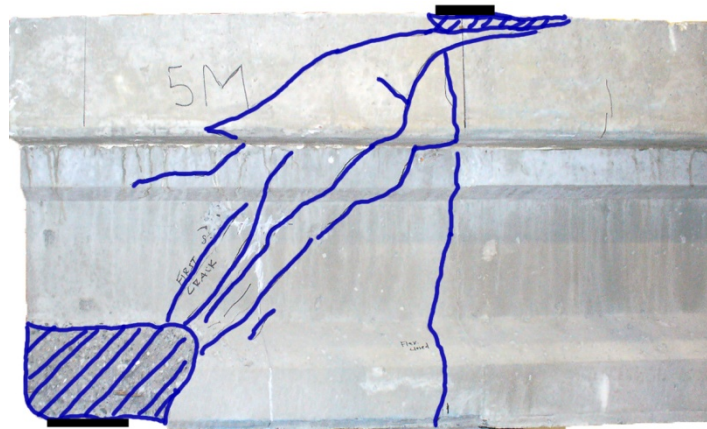
Figure 24–Bond-flexure failure mode (B5M-C)

6.3   B5S-C and B5S-U

Figure 25 summarizes the results from B5S-C and B5S-U. Each of these specimens had (4) 0.5-in. diameter strands, and varied only due to the presence or lack of confinement reinforcement. Both specimens behaved linear elastically until the formation of cracks. The first cracks were inclined web cracks occurring between the near support and the load point. Strain data from S2 gages indicated that initial cracks formed at applied loads of 105 kip and 113 kip for B5S-C and B5S-U, respectively. A flexural crack below the load point also formed in B5S-U at approximately 113 kip. As the load increased, additional cracks formed in each specimen, and

the cracks propagated into the flanges and the deck. Stiffness of each specimen was similar throughout loading.

Strands in each specimen began to slip after the formation of cracks. Strands in specimen B5S-C began to slip gradually at an applied load of 105 kip, and rapidly at load of 149 kip. Rapid slip at 149 kip corresponded to the formation of cracks within the development length. Strand slip in B5S-U was rapid, and began abruptly at load of 150 kip. Abrupt slip in B5S-U also accompanied the formation of a splitting crack above the near support at a load of 166 kip. The strand slip at maximum load was 0.34 in. and 0.07 in. for B5S-C and B5S-U respectively.

Specimen B5S-U supported as maximum applied load of 166 kip. At this load a splitting crack formed above the near support and the specimen almost instantly lost load capacity. Failure of B5S-U is designated as a splitting failure.

Splitting failure did not occur in B5S-C, allowing this specimen to support additional load and displacement beyond the point at which B5S-U failed. Absence of splitting in B5S-C is attributed to the confinement reinforcement which controlled formation of splitting cracks. By preventing splitting, the confinement reinforcement allowed larger loads to be developed in the top strand and vertical reinforcement, which added to the specimen capacity. Specimen B5S-C supported a maximum applied load of 199 kip. At this load, testing was terminated because the specimen had almost no stiffness. Continuation of the test would not have resulted in significantly higher load, but would have resulted in additional displacement, rotation, slip, and eventually crushing of the compression zone. Because B5S-C exceeded its nominal moment capacity, failure was categorized as a flexural failure. Figure 20 shows B5S-C after testing.
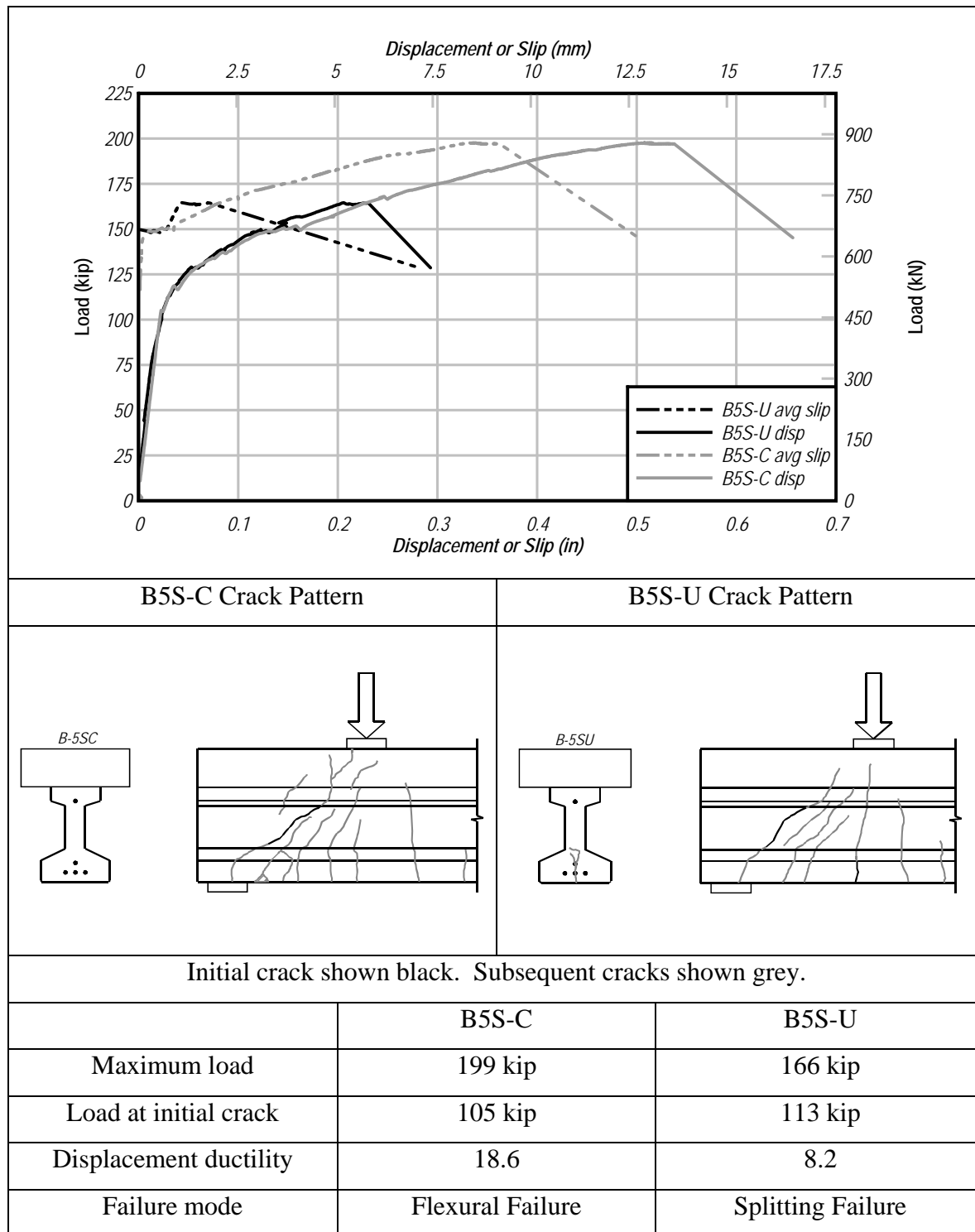
Figure 25– Summary of results for B5S-C and B5S-U

	B5S-C	B5S-U
Maximum load	199 kip	166 kip
Load at initial crack	105 kip	113 kip
Displacement ductility	18.6	8.2
Failure mode	Flexural Failure	Splitting Failure

6.4 B6L-C and B6L-U

Figure 26 summarizes test results from B5S-C and B5S-U. Each of these specimens had (6) 0.6 in. diameter strands, and varied only due to the presence or lack of confinement reinforcement. Both specimens behaved linear elastically until the formation of cracks. Inclined web cracks formed between the near support and the load point. Strain data from S2 gages indicate that initial cracks formed at applied loads of 114 kip and 134 kip for B6L-C and B6L-U, respectively. As the load increased, additional cracks formed in each specimen, and the cracks propagated into the flanges and the deck. Stiffness of each specimen was similar throughout loading. The post-cracking stiffness of these and the other B6 specimens was greater than the post-cracking stiffness of the B5 specimens.

Strands in each specimen began to slip after the formation of cracks. Strands in specimen B6L-C began to slip gradually at an applied load of approximately 140 kip, and more rapidly at an applied load of 179kip, after the formation of cracks within the development length. When compared to all other specimens, the strand slip in B6L-C occurred in more discrete events. The magnitude of the slip events increased with increasing load. Strands in B6L-U began to slip at 142 kip. Rapid strand slip in B6L-U accompanied the formation of a splitting crack above the near support at a load of 172 kip. The strand slip at maximum load was 0.12 in. and 0.02 in. for B6L-C and B6L-U respectively.

Specimen B6L-U supported as maximum applied load of 172 kip. At this load a splitting crack formed above the near support and the specimen almost instantly lost load capacity. Failure of B6L-U is designated as a splitting failure.

Splitting failure did not occur in B6L-C, allowing this specimen to support additional load and displacement beyond the point at which B6L-U failed. Absence of splitting in B6L-C is attributed to the confinement reinforcement which controlled formation of splitting cracks. By preventing splitting, the confinement reinforcement allowed larger loads to be developed in the top strand and vertical reinforcement, which added to the specimen capacity. B6L-C supported a peak applied load of 239 kip. Upon reaching 239 kip, the load dropped suddenly to approximately 220 kip. Testing continued after the peak load had been reached, with a series of load increases followed by sudden drops. The sudden drops in load corresponded to strand slip events. The test was terminated once it was apparent that the maximum load had been reached.

Failure of B6L-C (Figure 18) is designated as a bond-shear failure. The 239 kip load support by B6L-C is the largest load supported by any of the test specimens.

	B6L-C	B6L-U
Maximum load	239 kip	172 kip
Load at initial crack	114 kip	134 kip
Displacement ductility	6.3	1.6
Failure mode	Bond-Shear Failure	Splitting Failure
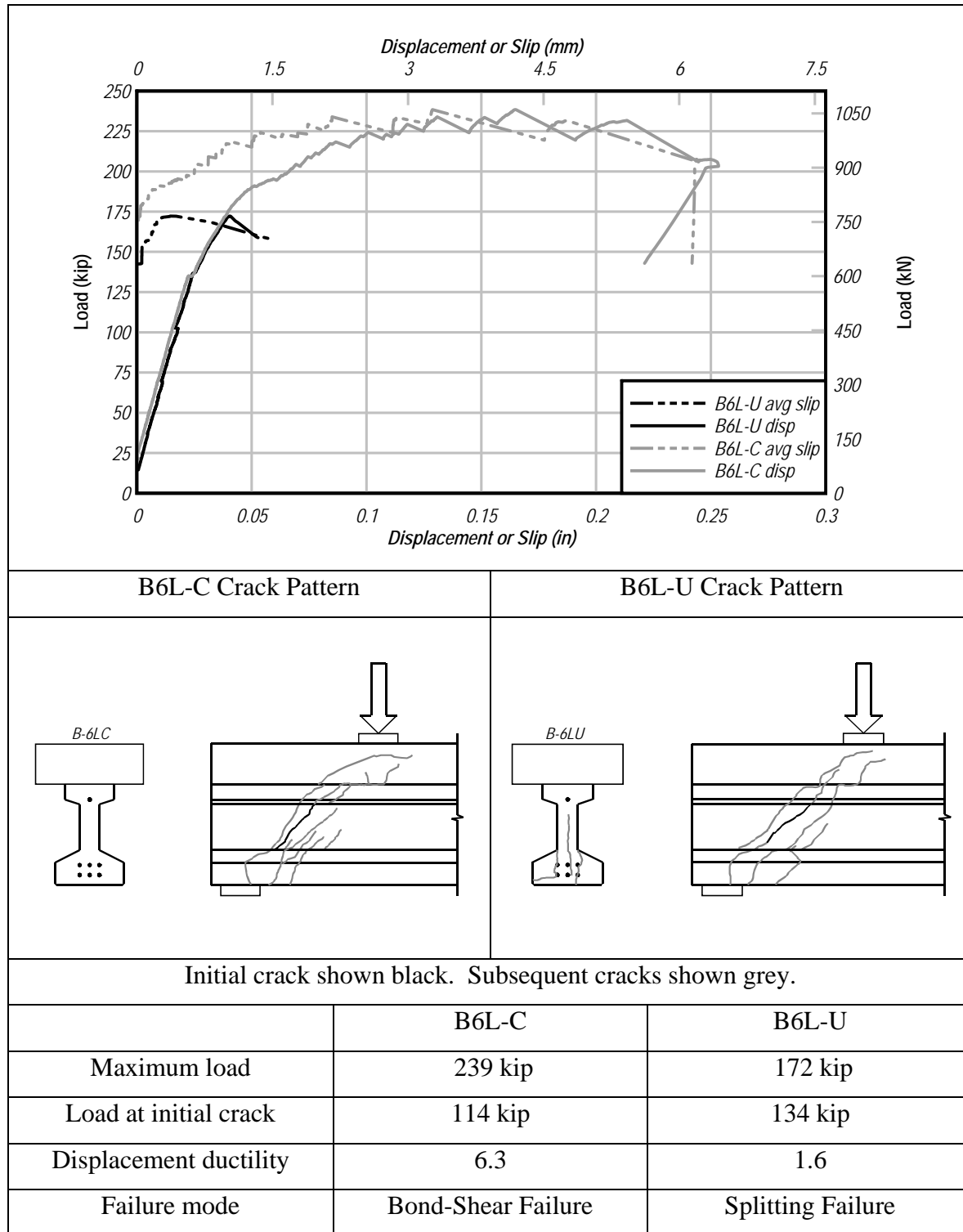
Figure 26– Summary of results for B6L-C and B6L-U

6.5 B6M-C and B6M-U

Figure 27 summarizes test results for B6M-C and B6M-U. Each of these specimens had (5) 0.6 in. diameter strands, and varied only due to the presence or lack of confinement reinforcement. Both specimens behaved linear elastically until the formation of cracks. The first cracks were inclined cracks occurring in the web between the near support and the load point. Strain data from S2 gages indicate that initial cracks formed at applied loads of 131 kip and 143 kip for B6M-C and B6M-U, respectively. As the load increased, additional cracks formed in each specimen, and the cracks propagated into the flanges and the deck.

The pre-cracking stiffness was almost identical for both specimens. However, the post-cracking stiffness of B6M-U could not be directly determined from the available data because the LVDT above the near support malfunctioned in the post-cracking phase of the test. To compensate for the lack of data, the bearing pad displacement at the near support was assumed to be 2.25 times the displacement of the bearing pad at the far support. The 2.25 factor is based on the ratio of the bearing pad displacements prior to the LVDT malfunction. The data presented in Figure 27 includes this assumption.

Strands in specimen B6M-U began to slip gradually at an applied load of about 80 kip, even before the formation of cracks. The 80 kip slip load was the lowest of any of the specimens. Strands in B6M-U began slipping more rapidly at load of 170 kip, after the formation of cracks in the bottom bulb. An abrupt slip event in B6M-U occurred at a load of 185 kip, and was association with the formation of splitting cracks at the end of the specimen. Strands in specimen B6M-C did not slip until a load of 156 kip, by which load an inclined crack had formed in the bottom bulb. The drops in load at 205 kip and 215 kip correspond to concrete spalling off the bottom bulb above the support. Spalling was limited to portions of the concrete outside of the confinement reinforcement. Strand slip at maximum load was 0.45 in. and 0.03 in. for B5M-C and B5M-U respectively.

Specimen B6M-U supported as maximum applied load of 185 kip. At this load a splitting crack formed above the near support and the specimen almost instantly lost load capacity. Failure of B6M-U (Figure 17) is designated as a splitting failure.

Splitting failure did not occur in B6M-C, allowing this specimen to support additional load and displacement beyond the point at which B6M-U failed. Absence of splitting in B6M-C is attributed to the confinement reinforcement which controlled formation of splitting cracks. By

preventing splitting, the confinement reinforcement allowed larger loads to be developed in the top strand and vertical reinforcement, which added to the specimen capacity. Specimen B6M-C supported a maximum applied load of 227 kip. At this load, the compression zone on either side of the load point crushed. The rotation that led to compression zone crushing was augmented by the strands slipping. Failure of B6M-C (Figure 19) is designated as a bond-flexure failure.
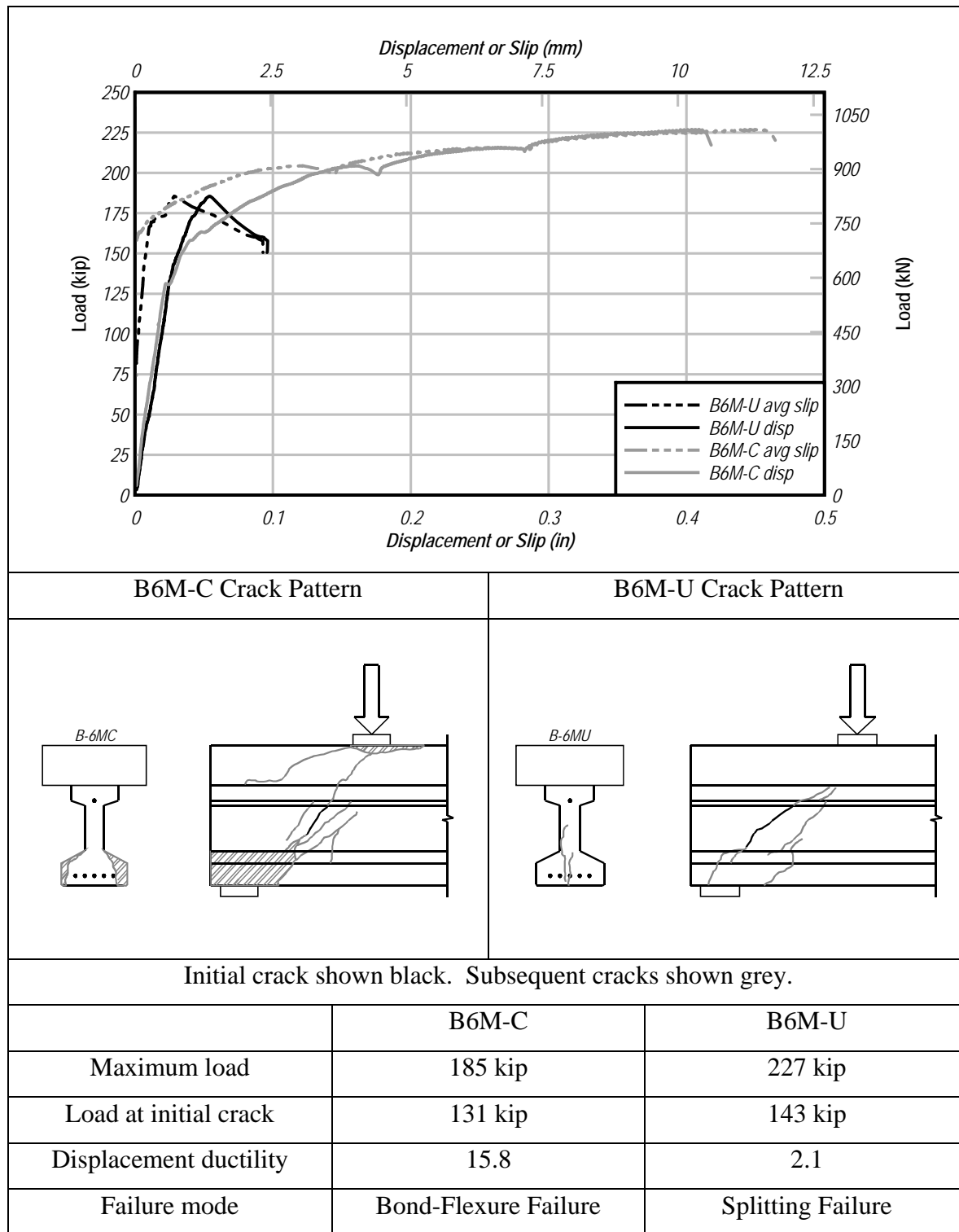
Figure 27– Summary of results for B6M-C and B6M-U

	B6M-C	B6M-U
Maximum load	185 kip	227 kip
Load at initial crack	131 kip	143 kip
Displacement ductility	15.8	2.1
Failure mode	Bond-Flexure Failure	Splitting Failure

6.6   B6S-C and B6S-U

Figure 28 presents a summary of test results for specimens B6S-C and B6S-U. Each of these specimens had (4) 0.6 in. diameter strands, and varied only due to the presence or lack of confinement reinforcement. Both specimens exhibited linear elastic behavior until the formation of cracks. The first cracks for both specimens were inclined cracks occurring in the web between the near support and the load point. Strain data from S2 gages indicate that the initial cracks formed at applied loads of 110 kip and 132 kip for B5S-C and B5S-U, respectively. As the load increased, additional cracks formed in each specimen, and the cracks propagated into the flanges and the deck. Stiffness of each specimen was similar throughout loading.

Strands in each specimen began to slip after the formation of cracks. Strands in specimen B6S-C began to slip gradually at an applied load of 130 kip and more rapidly at load of 157 kip, corresponding to the formation of a crack within the development length. Strand slip in B6S-U was rapid and began at load of 152 kip. The abrupt slip event in B6S-U at 154 kip accompanied the formation of a splitting crack above the near support. The strand slip at maximum load was 0.34 in. and 0.03 in. for B6S-C and B6S-U respectively.

Specimen B6S-U had the smallest capacity of any test specimen, supporting a maximum applied load of 154 kip. At this load a splitting crack formed above the near support and the specimen almost instantly lost load capacity. Failure of B6S-U is designated as a splitting failure.

Splitting failure did not occur in B6S-C, allowing this specimen to support additional load and displacement beyond the point at which B6S-U failed. Absence of splitting in B6S-C is attributed to the confinement reinforcement which controlled formation of splitting cracks. By preventing splitting, the confinement reinforcement allowed larger loads to be developed in the top strand and vertical reinforcement, which added to the specimen capacity. Specimen B6S-C supported a maximum applied load of 209 kip. At this load, testing was terminated because the specimen had almost no stiffness. Continuation of the test would not have resulted in significantly higher load, but would have resulted in additional displacement, rotation, slip, and eventually crushing of the compression zone. Failure of B5S-C (Figure 29) is designated as a bond-shear failure.
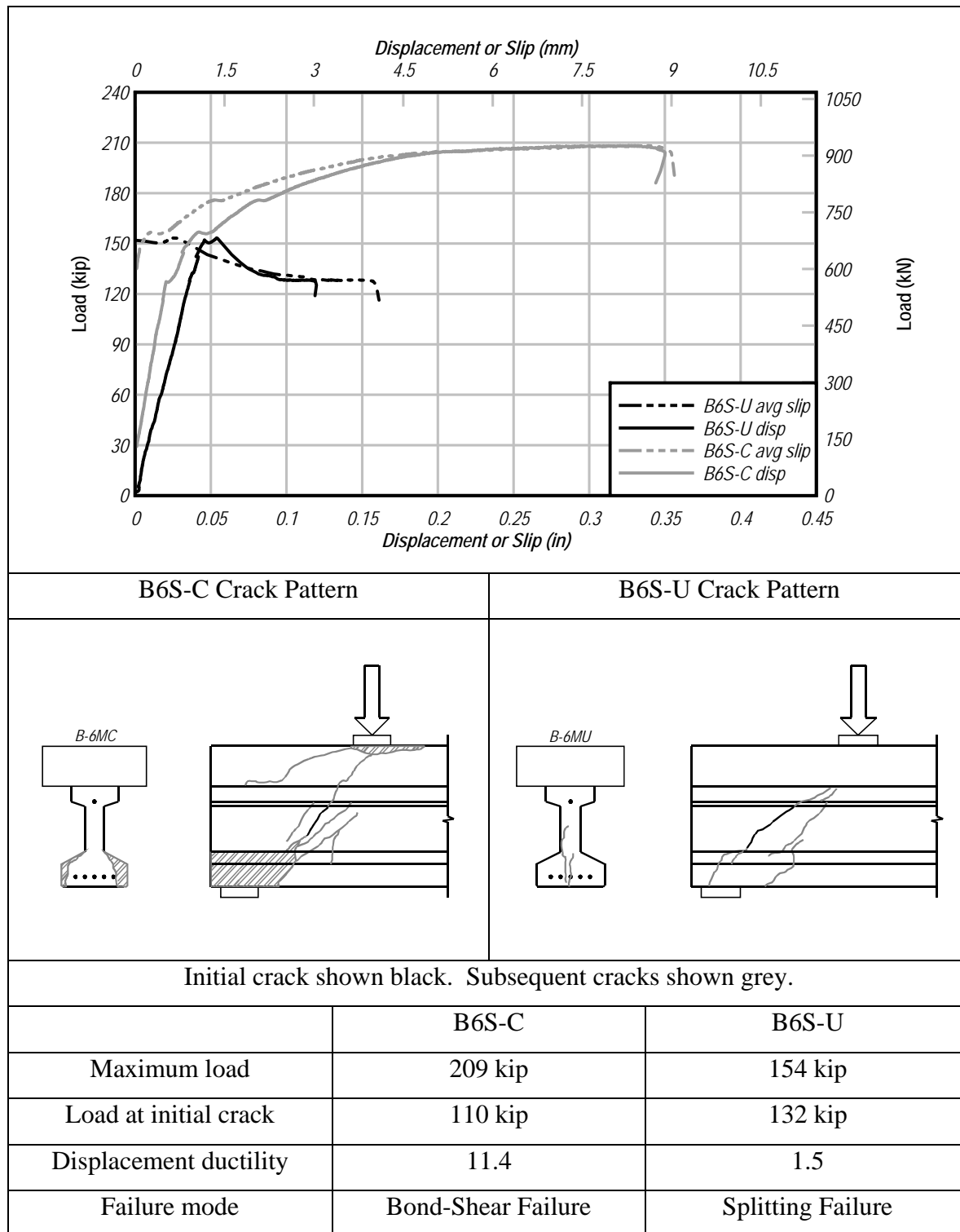
Figure 28– Summary of results for B6S-C and B6S-U

	B6S-C	B6S-U
Maximum load	209 kip	154 kip
Load at initial crack	110 kip	132 kip
Displacement ductility	11.4	1.5
Failure mode	Bond-Shear Failure	Splitting Failure
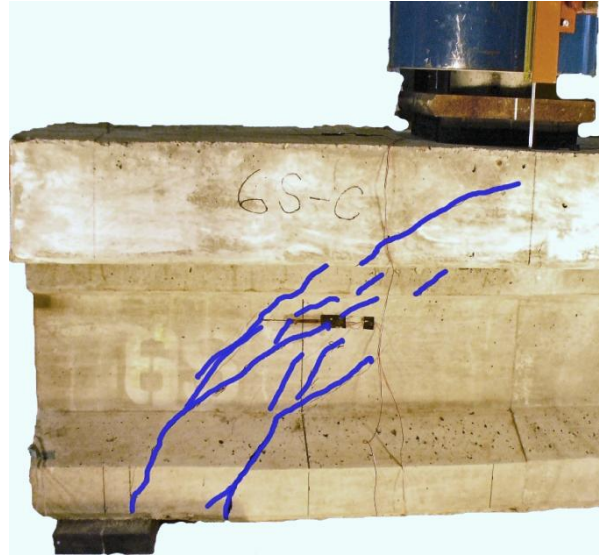
Figure 29– Bond-shear failure mode (B6S-C)

6.7 Transverse Strain

Strain gages were placed at the end of the specimens above the near support (Figure 15) to measure the transverse strain in the bottom flange. Figure 30 shows the strains reported by these gages at a load of 15 kip. This load was chosen because it was well within the linear-elastic range of all tests. Strain gages from each specimen reported that transverse strain was greatest below the web and decreased towards the edges of the flange. Figure 30 also shows the results of a finite element analysis which will be discussed in Appendix F.
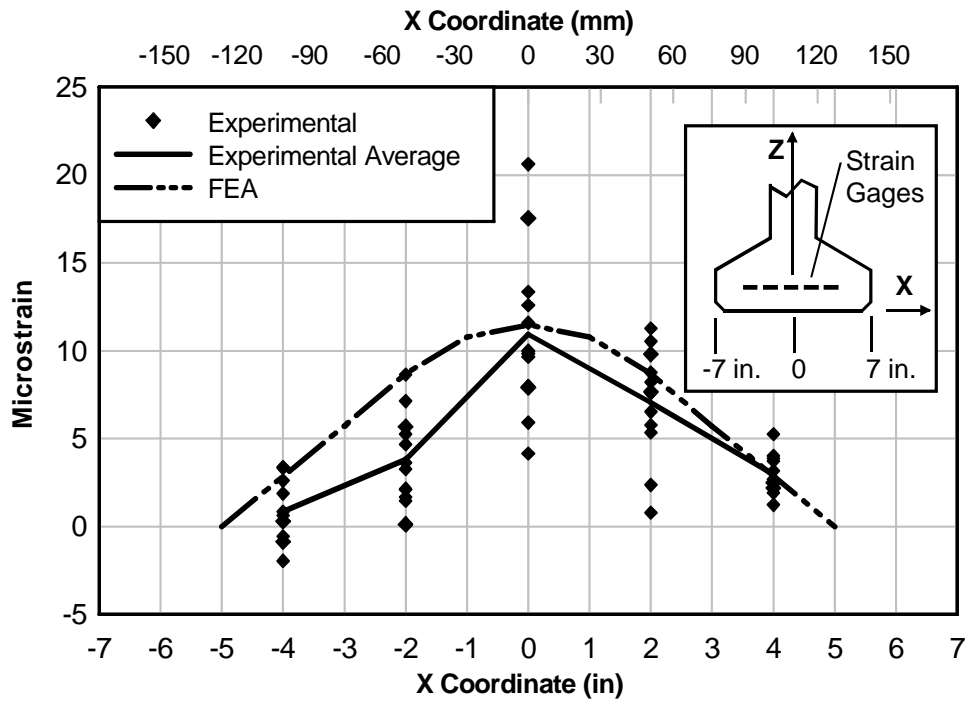
Figure 30–Transverse strain above near support (load =15 kip)

Figure 31 presents the superimposed shear versus transverse strain data from gages on the end of B6L-C. The trends in the figure are representative of all tests with confinement reinforcement. At the beginning of the test the strain was initially proportional to the applied load, indicating linear-elastic behavior. The strain-load relationship became nonlinear after the formation cracking in the web, and changed rapidly after the cracks propagated into the bottom flange and the strands began slipping. Splitting cracks were not visually observed in the confined specimens; however strain data suggest that a vertical splitting crack likely formed at the end of the confined specimens. This can be observed in Figure 31, where gage S8 reported a sudden increase in strain tensile strain at a load of approximately 190 kip. The magnitude of tensile strain reported by S8 is indicative of crack formation. Because of the confinement reinforcement, these cracks were controlled and splitting failure was prevented.
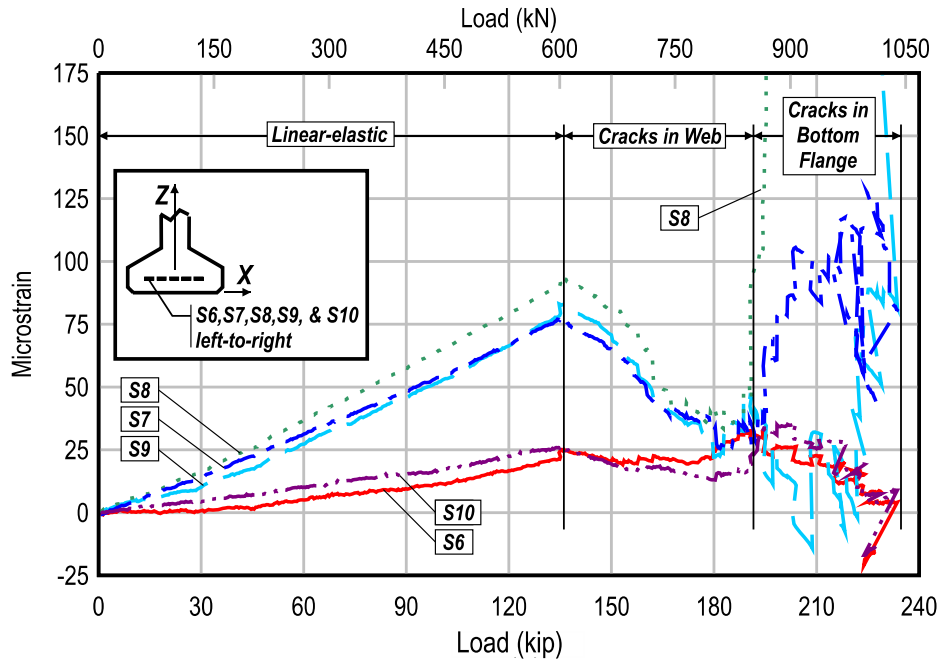
Figure 31–Effect of load on transverse strain in confined specimen (B6L-C).

Figure 32 presents the transverse strain data from gages on the end of B5L-U. Trends in this figure are representative of all unconfined tests. Strain was initially proportional to the applied load, indicating linear-elastic behavior. The strain-load relationship became nonlinear after the formation of cracks in the web. The strain changed rapidly after the cracks propagated into the bottom bulb, then again when splitting cracks formed.

Strain gage S4 was mounted transversely on the bottom on the specimens, approximately 5 in. in from of the bearing pad at the near support. Figure 33 shows load-strain data from gage S4 on B5M-C and B5M-U. The qualitative trends shown in the figure are representative of each pairing of confined and unconfined specimens. The load-strain relationship was initially linear for both the confined and unconfined specimens. The strain was compressive (negative) due to Poisson shortening in the transverse direction as the bottom of the specimen elongated in the longitudinal direction. Nonlinear behavior occurred with the formation of cracks at applied loads of 93 kip and 103 kip for B5M-C and B5M-U, respectively. Strain in B5M-U suddenly became increasingly tensile (positive) starting at a load of about 134 kip; indicating the formation of a crack near the gage location. The tensile strain continued to increase rapidly until splitting failure occurred at a load of 180 kip. For B5M-C, the strain reported by gage S4 continued to become increasingly more compressive (negative) as the load increased, even after the onset of

nonlinearity. Because transverse tensile strains did not occur in the confined specimen, the confinement reinforcement was thought to have prevented the propagation of splitting cracks near gage S4. This conclusion is supported by a visual examination of the specimen, which did not detect any splitting cracks at the end of B5M-C.
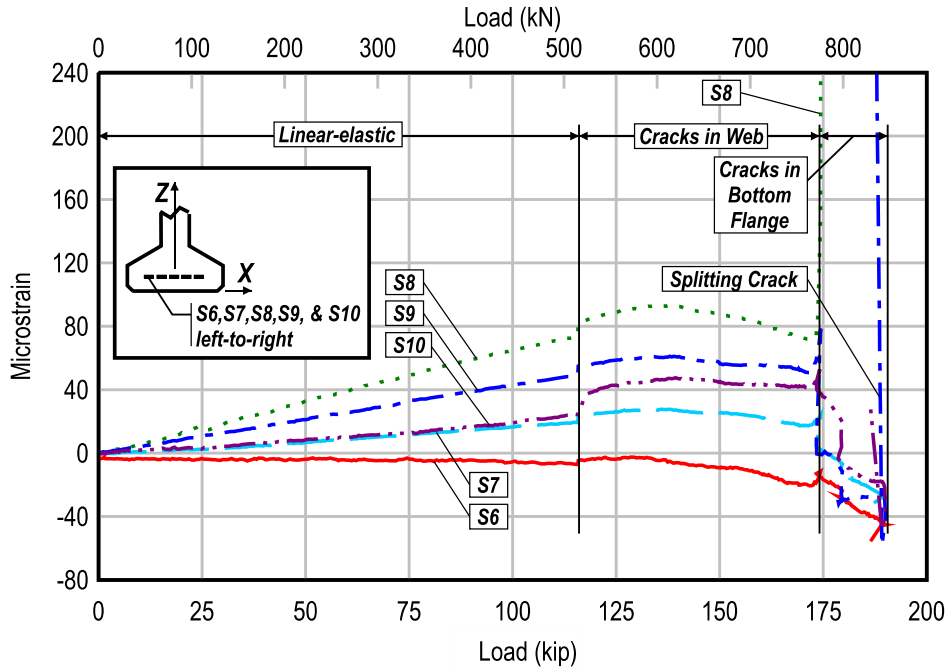
Figure 32–Effect of load on transverse strain in unconfined specimen (B5L-U)
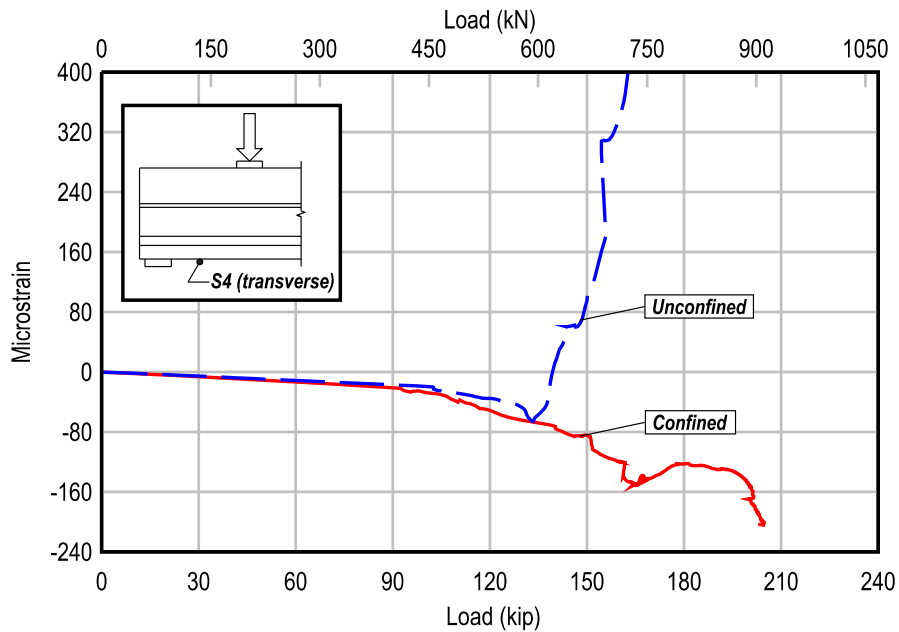
Figure 33–Strain readings from gage S4 (B5M)

6.8 Spalling: B5M-C and B6M-C

Edges of the bottom flanges of specimens B5M-C and B6M-C spalled off during testing. The spalling occurred above the near support, and was limited to the concrete outside of the confinement reinforcement. The confinement reinforcement was visible after the spalling, as shown in Figure 34.
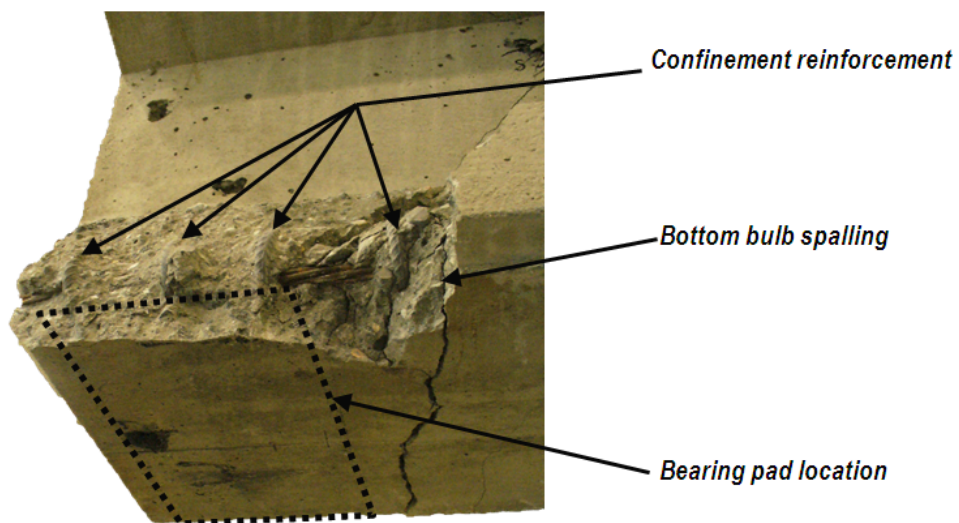
Figure 34–Flange spalling (B5M-C).

For both B5M-C and B6M-C, the load at which spalling occurred was similar to the load at which at which splitting cracks formed in the associated unconfined specimens B5M-U and B6M-U. This observation suggests that the confinement reinforcement had engaged and was supporting transverse forces that would have otherwise caused splitting in B5M-C and B6M-C. This observation is also consistent with the behavior of reinforcement concrete columns, where spalling is indicative that confinement reinforcement is engaged.

It is notable that spalling occurred in specimens B5M-C and B6M-C, both of which have five strands. The five strand layout placed strands near the edges of the bottom flange (Figure 6). Llanos et al (2009), reported that strand patterns with fully bonded strands placed at the edges of the flanges can lead to transverse splitting forces. These splitting forces in specimens B5M-C and B6M-C may have contributed load in the confinement reinforcement thereby leading to spalling. Another possible reason for the spalling in these specimens is that the concrete at the edges of the flanges were under greater compressive load due to the prestress force being applied by the outermost strands.

6.9   Individual Strand Slip

Strand slip data have been presented as the average slip of the bonded strands. Average slip is a convenient way of evaluating overall slip behavior, but load-slip data from individual strands is also instructive. Figure 35 presents the load-slip data for each strand in specimen B5S-C, and demonstrates general trends observed in the slip data from confined tests. Strand slip in B5S-C began gradually after the formation of cracks at load of approximately 120 kip, then increased rapidly as cracks propagated into the bottom bulb at approximately 145 kip. Each strand slipped at approximately the same load and through the same distance.
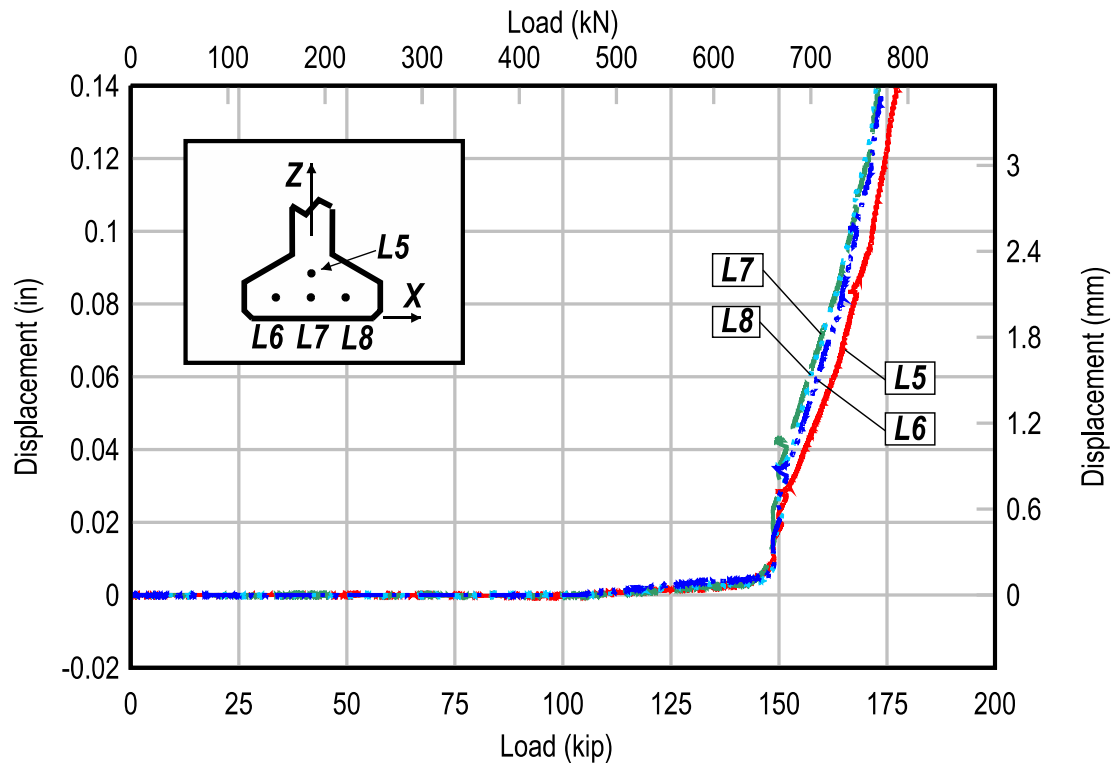
Figure 35–Prestressing strand slip in specimen B5S-C

Figure 36 shows the load-slip behavior for B5L-U, and demonstrates general trends observed in the slip data of the unconfined tests. Strand slip in the B5L-U occurred abruptly, and individual strands did not slip at the same load or through the same distance. The first strands to slip were those located at the centerline of the cross-section below the web. This can be seen in the figure, where strands 5 and 7 (located at the cross-section centerline) slipped first. Strands 6 and 8 were located away from the centerline and slipped later. An "unzipping" mechanism appears to have occurred in the unconfined specimens, where load was transferred to the outer strands after the inner strands began to slip. The outer strands also began to slip after the strand/concrete bond capacity was exceeded. All strands slipped when a splitting crack formed at the peak load of 166 kip.
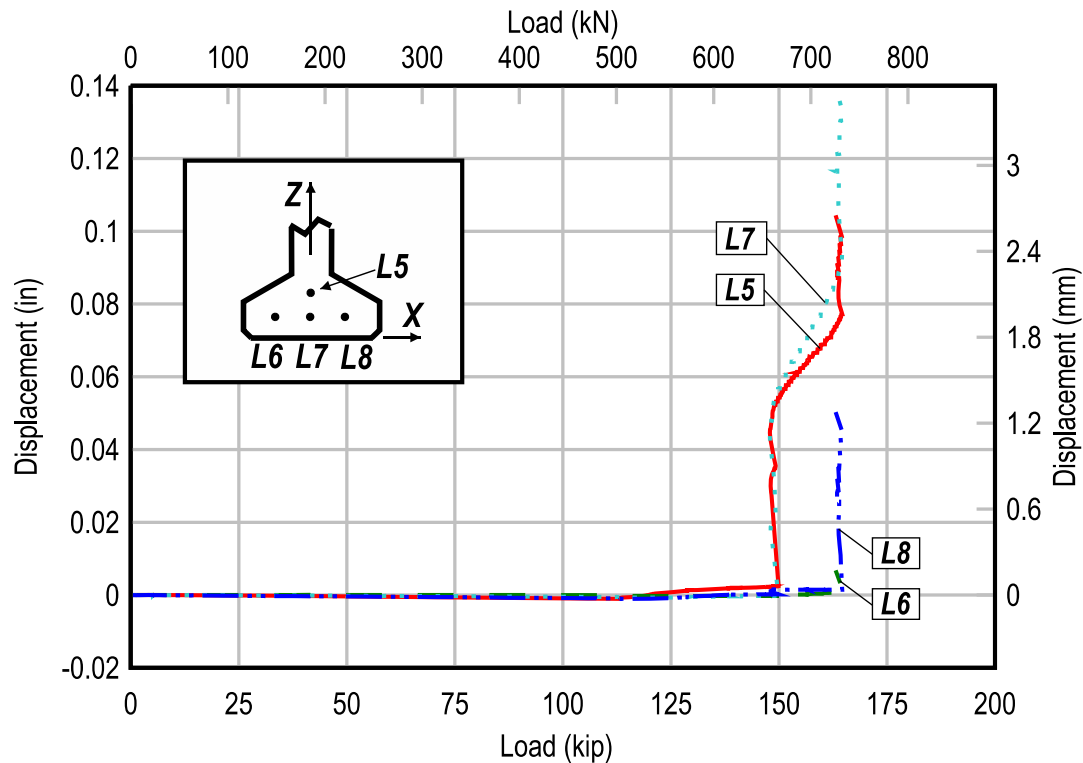
Figure 36–Prestressing strand slip in specimen B5S-U

Differences in load-slip behavior between the confined and unconfined specimens are attributed to the confinement reinforcement. Formation of cracks within the strand development length always preceded rapid strand slip. Cracks in the confined specimens engaged the confinement reinforcement, which then arrested the further propagation of cracking. Because crack propagation was hindered in the confined specimens, crack and slip events were initially less drastic than in the unconfined specimens. In addition to slowing crack propagation, confinement reinforcement is also believed to have created a confining force on the strands and concrete. By arresting the formation of cracks, and/or by providing a confining force, confinement reinforcement lead to more uniform conditions for the strands in confined specimens. This uniform condition is considered culpable for the observation that all strands in the confined specimen tended to slip together.

6.10 Shear Capacity

Figure 37 shows the normalized shear capacity for each test. Note that the shear capacity is taken as the shear force corresponding to the maximum load and occurring at the support

nearest the load point. Values have been normalized by the average of the unconfined specimen capacities, which was equal to 138 kip (614 kN). The data clearly indicate that variation in strand diameter had little effect on the shear capacity in unconfined tests. The average capacity of the unconfined tests with 0.5-in. (12.7 mm) diameter strand (B5 in the figure) and 0.6-in. (15.2 mm) diameter strand (B6 in the figure) varied by only 4%, indicating that strand size and area of prestressing steel did not significantly affect the capacity of the unconfined specimens.

Confined tests resulted in an average of 25% more shear capacity than that of the unconfined tests. Confinement reinforcement prevented splitting failure in the bottom flange, allowing the increased contribution from the vertical reinforcement. As the confined specimens rotated beyond the point at which the unconfined specimens split and failed, the forces in the vertical steel increased, leading to improvements in shear capacity. This presumption is supported by the load-displacement data from the confined specimens. The loss of stiffness as the confined specimens approached maximum capacity indicates that the vertical reinforcement and top strand were at or approaching yielding. The increased rotation also caused the resultant of the compressive force to move upwards in the section, thereby increasing the moment arm and shear contribution of the prestressing strands.
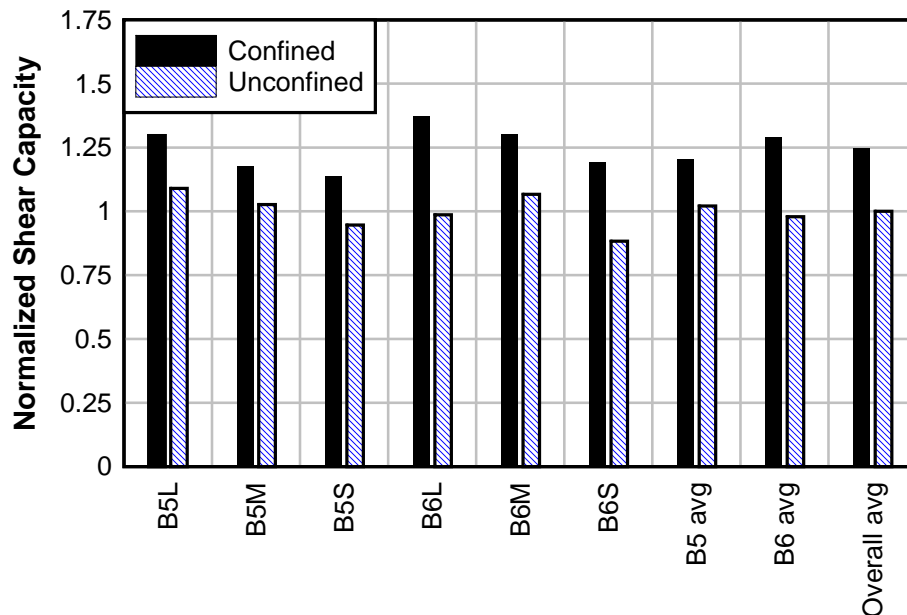
Figure 37–Normalized shear capacity

Figure 38 shows the shear capacity plotted against the area of prestressing steel for confined and unconfined tests. In the unconfined tests there is no clear relationship between shear capacity and area of prestressing steel, indicating that the capacity of the unconfined specimens was not a function the amount of prestressing steel. The confined tests, however, show a proportional relationship between the area of prestressing steel and the shear capacity. This difference is explained by the change in the nature of the failure mode with the addition of confinement reinforcement. In the tests with no confinement reinforcement, specimens reached capacity when end splitting occurred, which effectively eliminated strand bond at the end of the specimen. When confinement reinforcement was present, splitting failure was avoided and the prestressing strands were at least partially mobilized to contribute to shear capacity. This explains the direct proportionality between prestressing steel area and shear capacity in the confined tests.
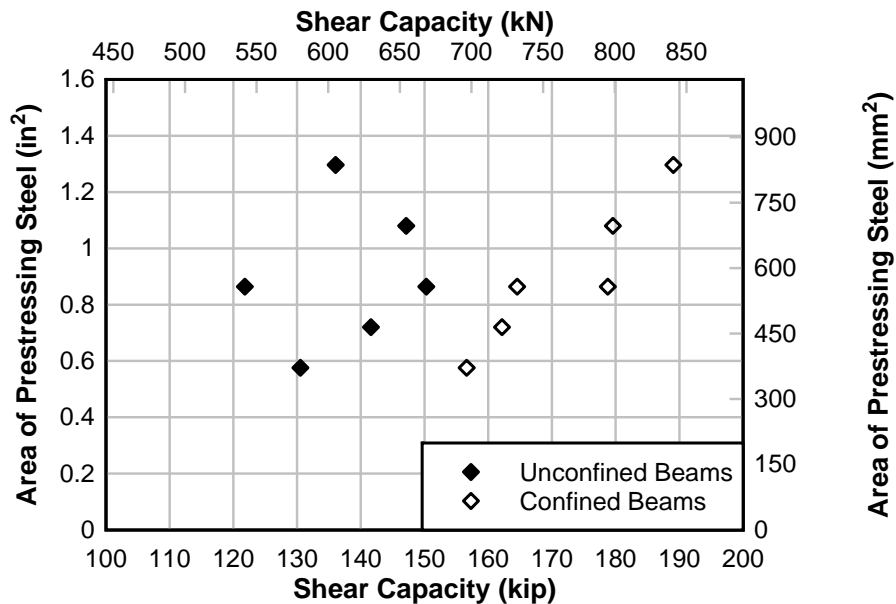
Figure 38–Effect of area of prestressing on shear capacity

6.11 Displacement Ductility

Figure 39 shows the displacement ductility for each specimen, normalized by the average ductility of all specimens. Displacement ductility was calculated by dividing the displacement occurring at maximum load by the displacement occurring at the onset of nonlinearity.

Displacement at maximum load was used in the calculations because the ultimate displacement was arbitrarily determined by the termination of the testing.

The average displacement ductility of the confined tests was 157% greater than that of unconfined tests. The greater ductility of the confined specimens is attributed to the confinement reinforcement, which prevented splitting failure and thereby allowed the confinement specimens to support larger displacements.
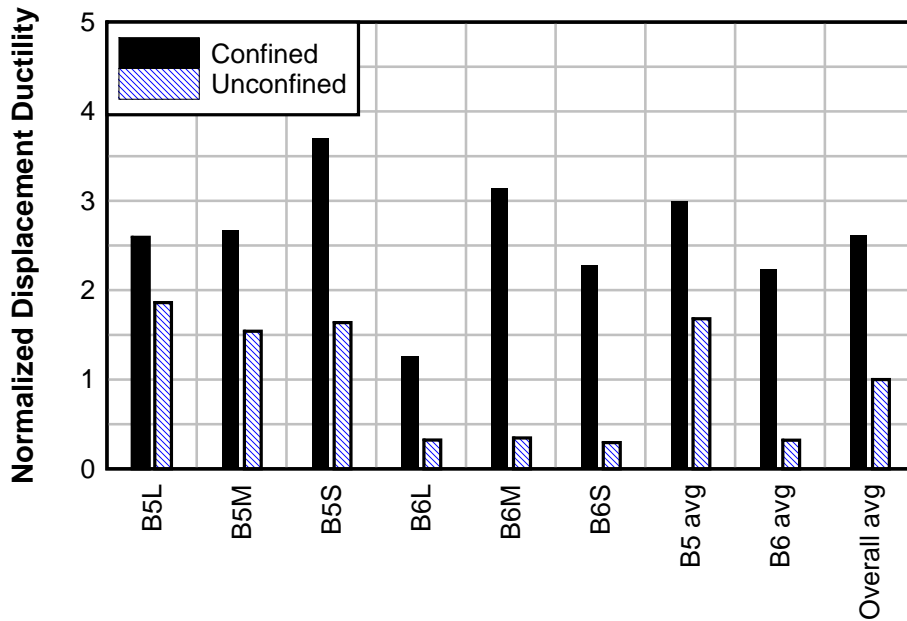
Figure 39–Normalized displacement ductility

7 Strut-and-Tie Model

Using an approach similar to the longitudinal reinforcement provisions in 5.8.3.5 of the 2007 AASHTO LRFD Bridge Design Specifications, strut-and-tie models (STM) were developed to describe the behavior and capacity of the unconfined and confined specimens. Models are presented in Figure 40 and Figure 41 for the unconfined and confined specimens, respectively. The only difference between the models is that the confined model considerers the confinement reinforcement to contribute in a manner similar to the vertical reinforcement (Csagoly, 1991). The STM models are based on a series of assumptions:

- A crack is assumed to form between the near support and the load point which crosses the bottom strands (T_1), top strand (T_2), vertical reinforcement (V_s), and confinement reinforcement if present ($V_{s,cr}$).

- The location of the compressive force, point 'C', was assumed to occur at the top of the beam. The STM shear capacity is derived from moment equilibrium about the point 'C'; point. Forces T_1, T_2, V_s, and $V_{s,cr}$ (confined specimens only), create moments about point 'C', and thus contribute to the shear capacity.

- Because the available development length of the bottom strands is shortened by the assumed crack, the bottom strands were assumed to be only 30% developed.

- The top strand and vertical reinforcement are fully developed.

- The assumed crack crosses (9) vertical bars. A smeared steel concept was used to place the combined effect of all vertical reinforcement at $a/2$.

- For the confined specimens, the crack was assumed to have engaged a single confinement hoop. Because the hoops are not long enough for full development, 75% development was assumed. The confinement reinforcement is assumed to act at the node directly above the bearing. Consideration of the confinement reinforcement as vertical reinforced was proposed by Csagoly (1991).

$$\Sigma M_C = 0 = -V_n a + T_1 d + V_s a/2 + T_2 d'$$

$$V_n = T_1 d/a + V_s/2 + T_2 d'/a$$
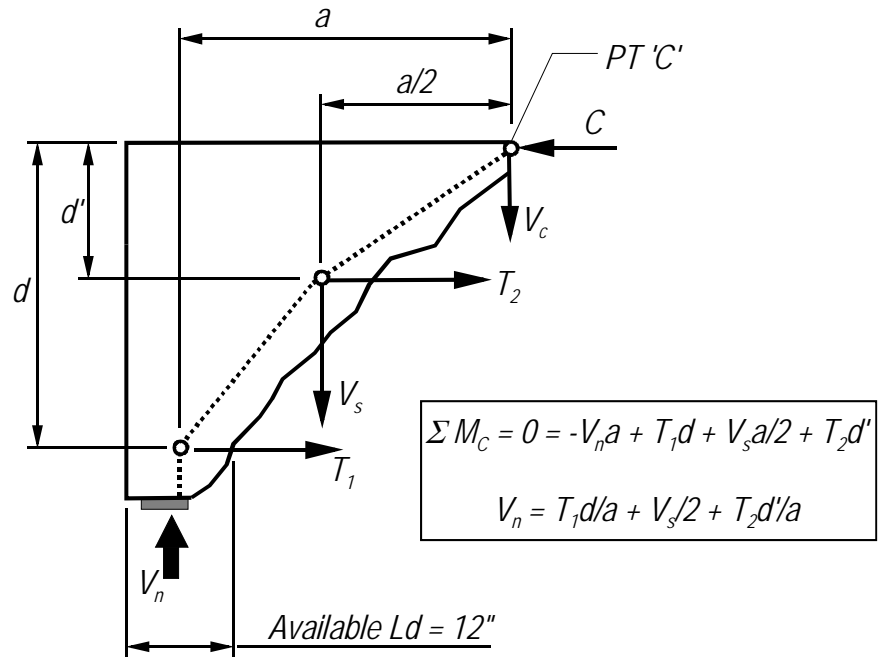
Figure 40–Unconfined specimen strut and tie model

$$\Sigma M_C = 0 = -(V_n - V_{s,cr})a + T_1 d + V_s a/2 + T_2 d'$$

$$V_n = T_1 d/a + V_s/2 + T2d'/a + V_{s,cr}$$
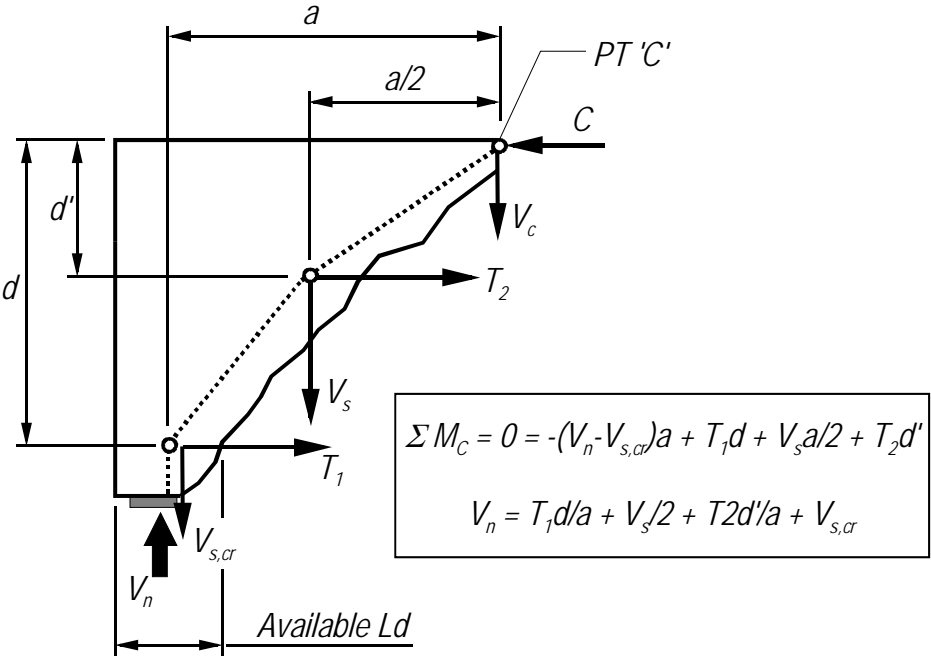
Figure 41–Confined specimen strut and tie model

STM predictions and experimental results are compared in Table 3. On average the STM predictions were within 3% of the experimental results. The STM always under-predicted the capacities of the specimens with 0.5 in. strands (B5), and over-predicted the capacities of

specimens with 0.6 in. strands (B6). Because the same strand development was used regardless of strand size, one possible reason for the difference is that the development was greater than the assumed 30% for B5 specimens and less than 30% for the B6 specimens. This rational is consistent with AASHTO LRFD section 5.11.4., which calculates development length as a function of strand diameter.

Another possible reason for the difference between the 0.5 in. and 0.6 in. strand specimens is that the top strand and mild reinforcement were less developed in the B6 specimens than in the B5 specimens. This is supported by the observation that the B6 specimens had smaller deflections at maximum load, suggesting that the steel in the B6 specimens may have been less developed than steel in the B5 specimens.

Table 3–Comparison of measured and computed shear capacity using STM

Test	V_{EXP} (kip)	V_{STM} (kip)	$\dfrac{V_{STM}}{V_{EXP}}$
B5L-C	167	181	1.09
B5L-U	149	152	1.02
B5M-C	155	164	1.06
B5M-U	137	144	1.05
B5S-C	142	159	1.12
B5S-U	124	133	1.07
B6L-C	208	191	0.92
B6L-U	190	138	0.73
B6M-C	191	182	0.96
B6M-U	173	149	0.86
B6S-C	173	167	0.97
B6S-U	155	124	0.80
Average			0.97
B5x Avg.			1.07
B6x Avg.			0.87
Bxx-C Avg.			1.02
Bxx-U Avg.			0.92

STM results are compared to the confined and unconfined tests results separately. Looking first at the unconfined tests, Table 4 lists the experimental results along with the STM calculated shear contribution of the top strand and vertical reinforcement. Even when calculated based on potentially unconservative assumptions (i.e. full development), the combined contribution of the top strand and vertical reinforcement do not account for the experimental

capacity. Thus the bottom strands were clearly contributing to the experimental shear capacity at peak load. The shear contribution of the bottom strands can be estimated by subtracting the shear contributions of the top strand and vertical reinforcement from experimental shear capacity. Estimated contributions of the bottom strands are listed in the final column of the table and demonstrate that the strands in the unconfined specimens contributed to the shear capacity up until the point of splitting failure.

Table 4–Estimated portion of shear carried by prestressing strand tie (unconfined specimens)

Test	Experimental shear capacity (kip)	STM shear contribution of vert reinf & top stand (kip)	Estimated shear supported by bottom strand contribution (kip)
	V_{EXP}	V_{VR+TS}	$V_{EXP} - V_{VR+TS}$
B5L-U	152	75	77
B5M-U	144	75	69
B5S-U	133	75	58
B6L-U	138	84	54
B6M-U	149	84	65
B6S-U	124	84	40

Looking now at the confined tests, the experimental results provide a means of evaluating the 30% bottom strand development assumed by the STM. An expression for force in the bottom strands (T_1) can be derived by rearranging the shear capacity equation in Figure 41. Using the derived expression, the bottom strand force can be estimated by substituting the experimental shear capacity (V_{EXP}) for the nominal shear capacity (V_n). An estimate for strand development can then be calculated by dividing the estimated bottom strand force by the ultimate strand capacity. These calculations are carried out in Table 5. The average estimated bottom strand development was calculated to be 32%, similar to the assumed 30%. Results of the calculations also support the previously discussed possibility that the 0.5 in. diameter strands were more developed than the 0.6 in. diameter strands.

Table 5–STM details of confined specimens.

Test	Exp. shear capacity (kip)	Shear contribution of vert. bars, confinement, & top stand (kip)	Estimated force supported by bottom strands (kip)	Ult. bottom strand capacity (kip)	Estimated development (%)
	V_{EXP}	$V_{VR+TS+CR}$	$T_{est} = (V_{EXP} - V_{VR+TS+CR})(a/d)$	T_{ult}	$(T_{est}/T_{ult})*100$
B5L-C	181	93	88	248	35
B5M-C	164	93	71	207	34
B5S-C	159	93	66	165	40
B6L-C	191	102	89	352	25
B6M-C	182	102	80	293	27
B6S-C	167	102	65	234	28
Avg.					32
Avg. B5					36
Avg. B6					27

The relationship between experimental shear capacity and area of prestressing steel provides yet another means of estimating the bottom strand development in the confined specimens. Figure 42 presents the experimental data and a trend line approximating the relationship between shear capacity and area of prestressing. The trend line is expressed mathematically in Equation 1. The area of prestressing strand (A_{ps}) is a variable in the linear term of Equation 1. Accordingly, the linear term is assumed to be the contribution to the shear capacity from the prestressing strands (Equation 2). For the tested a/d ratio of 1.0, the shear contribution of the bottom strands is equal to the force in the strands. Thus, the trend line implies that at maximum capacity, the bottom strands supported 80 ksi. This stress corresponds to 30% strand development, and is in good agreement with the assumed value.
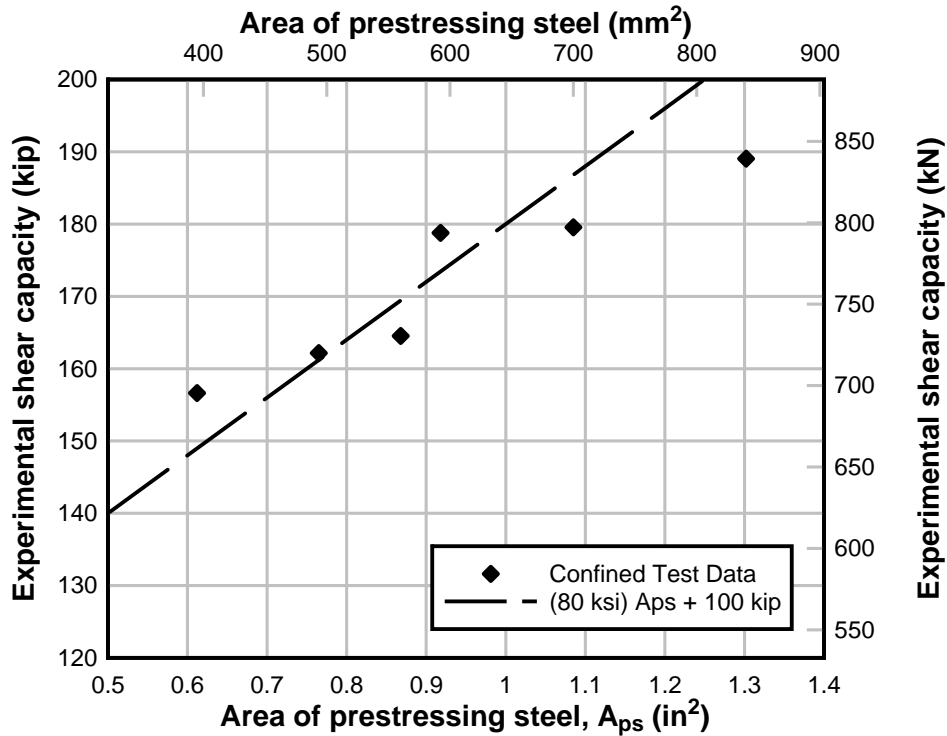
Figure 42–Experimental shear capacity vs. area of prestressing steel

$$V_{EXP} = A_{ps}(80ksi) + 100kip \qquad \text{Equation 1}$$

$$Bottom\ strand\ shear\ contribution = T_1\left(\frac{d}{a}\right) = A_{ps}(80ksi) \qquad \text{Equation 2}$$

The constant term in Equation 1 can also be related to the STM. Equation 3 assumes that the 100 kip constant term is equal to the combined shear contributions of the vertical reinforcement, top strand, and confinement reinforcement. Using the STM, the average combined contribution of these components was calculated to be 93 kip and 102 kip for the B5x and B6x specimens, respectively. The similarity between the experimental trend line and the STM suggests that the assumptions used in the STM are reasonable approximations of the physical system.

$$V_{VR+TS+CR} = 100kip \qquad \text{Equation 3}$$

8   Code Comparison

This section compares the experimental results with the nominal capacities calculated using current design codes. All calculations used the material properties shown in Table 6. The geometric properties, reinforcement, and prestressing were based on the specified values presented in section 3.

Table 6–Material properties used in calculations

Material Property	Value
Concrete deck compressive strength (Used in flexural calculations)	6500 psi
Concrete girder compression strength (Used for shear calculations)	8500 psi
Reinforcement yield strength	60 ksi
Prestressing strand ultimate strength	270 ksi

Experimental and code calculated shear capacities are presented in Table 7. Experimental results in the table include shear force due to the self-weight, as well as shear from the applied load. Nominal shear capacities were calculated using three methods:

1. Modified compression field theory (MCFT) from AASHTO LRFD Bridge Design Specification (2007).
2. Detailed method (ACI) from American Concrete Institute ACI 318 (2008).
3. Strut-and-tie modeling as presented in the previous section.

None of the specimens failed in the modes assumed by the MCFT and ACI calculations. Comparisons with these methods are nevertheless useful in evaluating the degree of conservatism in the code provisions. On average, MCFT was more conservative than ACI, predicting shear capacities that were only 75% of the experimental results. The ACI method predicted shear capacity to be 85% of the experimental results, on average.

Table 7–Comparison of calculated shear capacity with maximum experimental shear

Test	V_{EXP} (kip)	MCFT		ACI		STM	
		V_n (kip)	$\dfrac{V_{EXP}}{V_n}$	V_n (kip)	$\dfrac{V_{EXP}}{V_n}$	V_n (kip)	$\dfrac{V_{EXP}}{V_n}$
B5L-C	181	115	1.57	135	1.34	181	1.09
B5L-U	152	115	1.32	135	1.13	152	1.02
B5M-C	164	106	1.55	136	1.21	164	1.06
B5M-U	144	106	1.36	136	1.06	144	1.05
B5S-C	159	89	1.79	137	1.16	159	1.12
B5S-U	133	89	1.49	137	0.97	133	1.07
B6L-C	191	151	1.26	131	1.46	191	0.92
B6L-U	138	151	0.91	131	1.05	138	0.73
B6M-C	182	143	1.27	133	1.37	182	0.96
B6M-U	149	143	1.04	133	1.12	149	0.86
B6S-C	167	115	1.45	135	1.24	167	0.97
B6S-U	124	115	1.08	135	0.92	124	0.80
Average			1.34		1.17		0.97
Bxx-C Avg.			1.48		1.30		1.02
Bxx-U Avg.			1.20		1.04		0.92

The experimental bending moments were also compared with the capacities predicted by theory. Table 8 shows the maximum experimental moments as well as the nominal moment capacity predicted by strain compatibility. In all but one case, the specimens failed prior to reaching the nominal moment capacity. For test B5S-C, the experimental moment was 14% greater than the nominal moment capacity. This was specimens to have failed in flexure.

Table 8–Comparison of calculated moment capacity with maximum experimental moment

Test	M_{EXP} (kip-ft)	M_n (kip-ft)	$\dfrac{M_{EXP}}{M_n}$
B5L-C	431	488	0.88
B5L-U	362	488	0.74
B5M-C	390	427	0.91
B5M-U	343	427	0.80
B5S-C	379	333	1.14
B5S-U	317	333	0.95
B6L-C	455	673	0.68
B6L-U	329	673	0.49
B6M-C	433	594	0.73
B6M-U	355	594	0.60
B6S-C	398	472	0.84
B6S-U	295	472	0.63
Average			0.78
B*xx*-C Avg.			0.86
B*xx*-U Avg.			0.70

9   Summary and Conclusions

Twelve precast-prestressed test specimens were loaded to failure in three-point bending. The load point was placed approximately one member depth away from the support. Half of the specimens had confinement reinforcement and the other half did not. Other variables in the test program included the quantity and size of prestressing strands. The following conclusions are made:

- Confinement reinforcement had negligible effect on measured strain distribution prior to cracking.
- Transverse tensile strains formed in the bottom flange above the bearing pad. The maximum strain occurred at the centerline of the cross-section and the strain diminished to a minimum at the edge of the flange. Transverse tensile strains are believed to have led to splitting failures in the beams without confinement reinforcement.
- Confinement reinforcement did not consistently delay or prevent slipping of prestressing strands. Such reinforcement, however, did provide sufficient slip restraint to the strands to ensure that they were able to continue supporting tensile forces beyond the point at which the unconfined test specimens failed.
- Confinement reinforcement prevented splitting failure, thereby improving the shear capacity and displacement ductility of the confined tests relative to the unconfined tests. Average shear capacity increase was 25% and the average increase in displacement ductility was 157%.
- Experimental results and strut-and-tie modeling suggest that the strands were 30% developed on average at peak load. Development of the strands in the experimental tests was limited by the formation of cracks within the strand development length.